# *Investigating the impacts of COVID-19 lockdown on air quality, surface Urban Heat Island, air temperature and lighting energy consumption in City of Melbourne*

Energy Strategy Reviews 44 (2022) 100963

Contents lists available at ScienceDirect

Energy Strategy Reviews

journal homepage: www.elsevier.com/locate/esr

# Investigating the impacts of COVID-19 lockdown on air quality, surface Urban Heat Island, air temperature and lighting energy consumption in City of Melbourne

Elmira Jamei [a], Yashar Jamei [b,*], Mehdi Seyedmahmoudian [c], Ben Horan [b], Saad Mekhilef [c], Alex Stojcevski [c]

[a] College of Engineering and Science, Victoria University, Melbourne, Victoria, Australia
[b] School of Engineering, Deakin University, Geelong, Victoria, Australia
[c] School of Software and Electrical Engineering, Swinburne University of Technology, Melbourne, Victoria, Australia

ARTICLE INFO

*Keywords:*
COVID-19 pandemic
Energy consumption
Air pollution
Land surface temperature
Google earth engine

ABSTRACT

The COVID-19 pandemic has threatened city economies and residents' public health and quality of life. Similar to most cities, Melbourne imposed extreme preventive lockdown measures to address this situation. It would be reasonable to assume that during the two phases of lockdowns, in autumn (March) and winter (June to August) 2020, air quality parameters, air temperature, Surface Urban Heat Island (SUHI), and lighting energy consumption most likely increased. As such, to test this assumption, Sentinel 5, ERA-5 LAND, Sentinel 1 and 2, NASA SRTM, MODIS Aqua and Terra, and VIIRS satellite imageries are utilized to investigate the alterations of $NO_2$, $SO_2$, CO, UV Aerosol Index (UAI), air temperature, SUHI, and lighting energy consumption factors in the City of Melbourne. Furthermore, satellite imageries of SentiThe results indicate that the change rates of $NO_2$ (1.17 mol/$m^2$) and CO (1.64 mol/$m^2$) factors were positive. Further, the nighttime SUHI values increased by approximately 0.417 °C during the winter phase of the lockdown, while during the summer phase of the lockdown, the largest negative change rate was in $NO_2$ (−100.40 mol/$m^2$). By contrast, the largest positive change rate was in $SO_2$ and SUHI at night. The $SO_2$ values increased from very low to 330 μm mol/$m^{2,}$ and the SUHI nighttime values increased by approximately 4.8 °C. From the spatial point of view, this study also shows how the effects on such parameters shifted based on the urban form and land types across the City of Melbourne by using satellite data as a significant resource to analyze the spatial coverage of these factors. The findings of this study demonstrate how air quality factors, SUHI, air temperature, and lighting energy consumption changed from pre-lockdown (2019) to lockdown (2020), offering valuable insights regarding practices for managing SUHI, lighting energy consumption, and air pollution.

## 1. Introduction

In recent years, rapid urbanization has resulted in a significant increase in anthropogenic heat released from human metabolism and transportation. Consequently, energy usage in different sectors, mainly housing, has increased, resulting in rapid alterations in the urban climate. Urbanization has also contributed to land cover types and energy balance changes, particularly in dense urban areas. Land cover alterations and their radiative and thermal properties play an important role in Land Surface Temperature (LST), air temperature values, and spatial pattern alterations. For instance, low vegetation coverage could decrease evaporative cooling and increase the emitted heat from other types of urban infrastructure. Meanwhile, LST and air temperature increment could intensify the energy consumption in buildings due to air conditioning systems being used by building residents [2].

Moreover, LST and air temperature alteration are related to the anthropogenic heat release caused by humans and their vehicles, resulting in air pollution in the forms of Carbon Dioxide ($CO_2$), Nitrogen Dioxide ($NO_2$), Sulfur Dioxide ($SO_2$), and other types of aerosols [3–5]. The trade-off between temperature change (LST and air temperature) and air pollution is more substantial during the hot summer and cold

* Corresponding author.
*E-mail addresses:* elmira.jamei@vu.edu.au (E. Jamei), y.jamei@deakin.edu.au (Y. Jamei), mseyedmahmoudian@swin.edu.au (M. Seyedmahmoudian), ben.horan@deakin.edu.au (B. Horan), smekhilef@swin.edu.au (S. Mekhilef), astojcevski@swin.edu.au (A. Stojcevski).

https://doi.org/10.1016/j.esr.2022.100963
Received 18 November 2021; Received in revised form 15 August 2022; Accepted 6 September 2022
Available online 8 September 2022

**Abbreviations**

| | |
|---|---|
| UHI | Urban Heat Island |
| CBD | Central Business District |
| Amount of lighting | Lighting accounts for around 10% of electricity usage in households and 18%–40% of usage in commercial premises [1] https://www.energyrating.gov.au/products/lighting#:~:text=Overview |
| RS | Remote Sensing |
| VIIRS | Visible Infrared Imaging Radiometer Suite |
| GHG | Green House Gases |
| WHO | World Health Organization |
| $W/m^2$ | Watt per square metre |
| LGA | Local Government Area |
| SA2 | Statistical areas (2) |
| TROPOMI | Tropospheric Monitoring Instrument |
| ECMWF | European Centre for Medium-Range Weather Forecasts |
| GEE | Google Earth Engine |
| SAR | Synthetic Aperture Radar |
| GRD | Ground Range Detected |
| MSI | Multispectral Instrument |
| DEM | Digital Elevation Model |
| NRTI | Near Real Time |
| NDVI | Normalized Difference Vegetation Index |
| MNDWI | Mean Normalized Difference Water Index |
| DNB | Day/Night Band |
| NOAA | National Oceanic and Atmospheric Administration |
| NCEI | National Centers for Environmental Information |
| NTL | Nighttime Lights |
| NDBI | Normalized Difference Built-up Index |
| $CO_2$ | Carbon Dioxide |
| $NO_2$ | Nitrogen Dioxide |
| $SO_2$ | Sulfur Dioxide |

winter days/months of the year. During the summer months, the heat and radiation in the sunlight lead to the combination of the ozone and other pollutants, such as $NO_2$, resulting in poor air quality. During winter, pollutants cannot escape and disperse in the dense colder air, which moves slower than warm air and could trap the pollutants. Energy consumption and air pollution have an influence on one another. Today, compulsory building regulations, standards, and retrofits reduce buildings' energy consumption, which could significantly minimize the need for power generation. Similarly, improvements in industrial site efficiency could result in significant emission reductions from fossil fuel-based power generation [6].

Understanding the relationship between human activity and the factors described above can be difficult due to the complexity of isolating various inputs. Doing so also involves evaluating the impact of meteorological conditions and the variations in built forms and land use across geographical areas. However, an opportunity to explore this with greater clarity has arisen unexpectedly due to the COVID-19 pandemic.

The coronavirus, later designated "COVID-19", first emerged in late 2019 in Wuhan City, Hubei Province, China and was then declared a pandemic by the World Health Organization (WHO) on March 11, 2020. COVID-19 is an extremely transmissible virus that caused more than 14,000 deaths and 334,000 infections by March 23, 2020 [7]. By April 26, 2020, the death rate had reached 200,000 globally.

In response, governments implemented strict measures to reduce the frequency and duration of face-to-face interactions and social gatherings to slow down the spread of the virus. These measures substantially changed the environment lighting energy consumption of the cities and the pattern of human activities. For example, drastic reductions were observed in the industrial (35%) and transportation activities (50%) in the San Francisco Bay area during a COVID-19 lockdown [8]. Some changes brought permanent alterations to urban areas (e.g. rededicating street space for pedestrians and cyclists and working from home arrangements even after COVID-19).

Many methods and models are available to study Urban Heat islands (UHIs), temperature alteration, air pollution, and energy consumption in cities. Those focused on addressing the spatial variations of the above-mentioned factors have gradually improved to address the challenges posed by their coarse spatial and limited temporal resolution, which underestimate the temperature variation, especially in highly dense urban areas where anthropogenic heat emissions are maximized [9]. Remote Sensing (RS) is an ideal tool to capture and monitor the temperature, UHI, and air pollution at the fine spatial scale and assist scholars in characterizing the spatial variation of UHIs better. However, this exercise is only feasible under clear sky conditions [10].

The current study focuses on altering air pollution, air temperature, Surface Urban Heat Island (SUHI) and lighting energy consumption during pre-lockdown and lockdown phases in the City of Melbourne, Victoria, Australia. By September 1, Australia's death rate had reached 576, while 19,224 COVID-19 cases were confirmed [11]. Similar to other citieis in Australia, Lockdowns in various phases were declared in Melbourne on March 26, 2020. They initially lasted for more than 250 discontinuous days until July 31, 2021. Consequently, more than 1.3 million Victorians stayed home during this period. A report provided by the Victoria state government Department of Health [12] acknowledges that around 75% of Melbourne's air pollution is because of vehicle emissions caused by petroleum combustion and the burning of other fuels (such as gas, wood, and coal). The burning gases include CO, nitrous oxide, and particulates. When Melbourne faces light winds or stable conditions, it will more frequently suffer from air pollution. The comparison between Melbourne suburbs shows that those receiving sea breezes and that are located close to coastal areas have better air conditions. Furthermore, low-lying areas will have worse air conditions than hilltop areas because pollutants tend to settle in valleys, especially on calm nights. According to the Victoria state government Department of Health report [12], the major forms of air pollution are summer and winter smog, windblown dust, and smoke. During the summer days, smog arises due to the effect of sunlight on airborne chemicals, resulting in the production of photochemical oxidants. Winter smog appears when pollutants build up around the city and are not blown away. In the current study, Landsat 8, Sentinel 5, ERA 5-Land, Visible Infrared Imaging Radiometer Suite (VIIRS), and MODIS satellite imageries and databases were used at the city level in the City of Melbourne to provide information on the impact of the COVID-19 pandemic on urban temperatures, SUHI, air pollution, and lighting energy consumption.

To our knowledge, this study is the first to assess the direct impact of COVID-19 on factors in the City of Melbourne. Previous studies on the environmental effects of COVID-19 have mainly focused on aerosols, Green House Gases (GHG), LST, and other pollutants, such as $NO_2$, in different cities across the globe [13–15]. Studies on the effect of COVID-19 lockdowns are limited, meaning reduced human activities, such as energy and lighting consumption and its trade-off with LST, air temperature, SUHI, and air quality parameters underexplored. Studies in the literature could be classified into three main topics considering this research's main focus: (1) SUHI, human activity, and pandemic lockdowns [16–25]. For instance, in the study conducted in Melbourne by Wai et al. [34], authors mentioned that the UHI intensity was 1 °C lower than the past five year's averages during the July to August month (Winter lockdown). This situation shows that the weekly cycle of anthropogenic activity and pollution could influence the UHI significantly [35,36]. (2)Air quality and pandemic lockdowns [26–33]. For

example, Ryan, et al. [49] estimated the air quality and health impact of the 2019–20 Black Summer megafires and COVID-19 lockdowns in Melbourne and Sydney, Australia. The authors utilized a meteorological normalization approach (Random Forest (RF) machine learning algorithm) to exclude the effect of meteorological parameters. Ryan et al. [50], stated that wind speed impacts air quality. This study also demonstrated that the machine learning predictions provided a baseline for examining the impact of the COVID-19 restrictions on air quality. The authors also presented two-and-a-half years of measurements of $NO_2$, formaldehyde (HCHO), glyoxal (CHOCHO), and Ozone ($O_3$) in Melbourne, Australia. Finally, (3) Energy consumption and pandemic lockdowns [34–39]. These studies are generally indicating that anthropogenic heat exacerbates SUHI and air pollution and increases air and surface temperature in Central Business District (CBD)s by several degrees Celsius (depending on the location and time of the year), thereby affecting the energy consumption rate (particularly lighting) in summer and winter.

As such, lockdowns such as th pose experienced in Melbourne could potentially positively affect urban areas' environment, ranging from improved air quality to reduced anthropogenic heat generation, as air pollution is the major contributor to urban overheating. The unprecedented situations arising from the pandemic provide an opportunity to explore whether specific urban planning policies can contribute to effective adaptation and mitigation of climate change.

In summary, this study aims to investigate the effect of lockdown in Melbourne CBD on the air temperature variation, air quality, SUHI, and lighting energy consumption. Accordingly, the summer (March) and winter (June to August) months during lockdown were considered to further investigate these factors.

The objectives of this study are as follows:

1. To investigate the descriptive statistical status of air quality factors ($NO_2$, $SO_2$, CO, and UV Aerosol Index (UAI)), air temperature, SUHI, and lighting energy consumption during the summer and wintertime pre-lockdown (2019) and during lockdown (2020) in the City of Melbourne.
2. To analyze the spatial distribution of air quality factors ($NO_2$, $SO_2$, CO, and UAI), air temperature, SUHI and lighting energy consumption during the summer and wintertime pre-lockdown (2019) and during lockdown (2020) in the City of Melbourne
3. To understand the most significant change rate considering air quality factors during pre-lockdown (2019) and lockdown (2020).

## 2. Methodology

### 2.1. Study area

The area selected for study was the City of Melbourne (Fig. 1b and c), which is a Local Government Area (LGA) of Melbourne located within the broader area of Greater Melbourne (Fig. 1a)in "-37.81753º N" <> "37.81753º S". . Melbourne CBD is located between −37.81753° N and 144.96715° E. The elevation range of the study area ranges from −100 m to 200 m, including coastal areas in the southern part of the city (Fig. 1b and c). The City of Melbourne municipality covers 37.7 $km^2$ and has a residential population of almost 184,000 (as of 2020). The area contains the central business district (CBD) in the city center and a number of inner suburbs that have distinctive characteristics, a range of businesses and dwellings, and a variety of communities living and working within them. Furthermore, approximately 972,000 people, on average, use the city during weekdays [40]. Melbourne has a temperate oceanic climate, hot summers, and mild winters (Köppen Climate Classification) [41]. The Köppen–Geiger climate classification in Melbourne


**Fig. 1.** (a) Greater Melbourne area, its LGAs and suburbs; (b) City of Melbourne aerial image; (c) City of Melbourne Statistical areas (2) (SA2) boundaries.

is 'CFB,' which can be described as warm temperate, fully humid, and warm summer. Melbourne's average maximum and minimum temperature values during summer are 25 °C and 14 °C, respectively. Meanwhile, the maximum and minimum temperature values during the wintertime are 14 °C and 7 °C, respectively [40].

The City of Melbourne was selected as a case study for this research because it is an ideal representative of the different types of urban forms, land covers, travel modes, and anthropogenic heat as it is the destination of many people from other areas of Melbourne to work, study, and enjoy recreation. CBDs are the heart of economic, political, recreational, cultural, and innovation activities In addition, Melbourne CBD was the area most impacted by COVID-19 lockdowns (over 70% of people have stopped or are visiting less) [42]. Online reports [43,44] have indicated that various industries and public services might face decentralization from the CBD due to the impact of COVID-19 lockdowns and that the goal of a 20-min neighbourhood could be achieved in Melbourne CBD. An examination of the City of Melbourne as a case study regarding this study's key factors could give city planners valuable ideas for formulating mitigation strategies and designing implementation as they strive for these goals and adjust to a new reality.

### 2.2. Datasets description

The datasets and satellite imageries used in this study were analyzed within the pre-lockdown (2019) and lockdown (2020) phases in non-consecutive days of the summer month of March and the winter months of July to August. The first lockdown started on March 26, 2020, in Melbourne, and the second one was from July 9 until October 27. Accordingly, only the available data during these months were considered for the summer and winter seasons. For instance, the focus on the available data during the winter season was between July and August. Given that the meteorological parameters are key factors affecting air pollution concentrations [45], the details regarding the general meteorological parameters, such as daily temperature, humidity, rainfall, and wind speed, at the Melbourne Olympic Park weather station (as a the key representative of the City of Melbourne meteorological status) are presented in Fig. 2. Furthermore, the databases and satellite imageries utilized in this study are provided in Table 1.

The air quality factors were measured by the Sentinel-5p Tropospheric Monitoring Instrument (TROPOMI) mission of Copernicus ESA with a spatial resolution of 3.5 × 7 $km^2$ [54]. The average monthly and

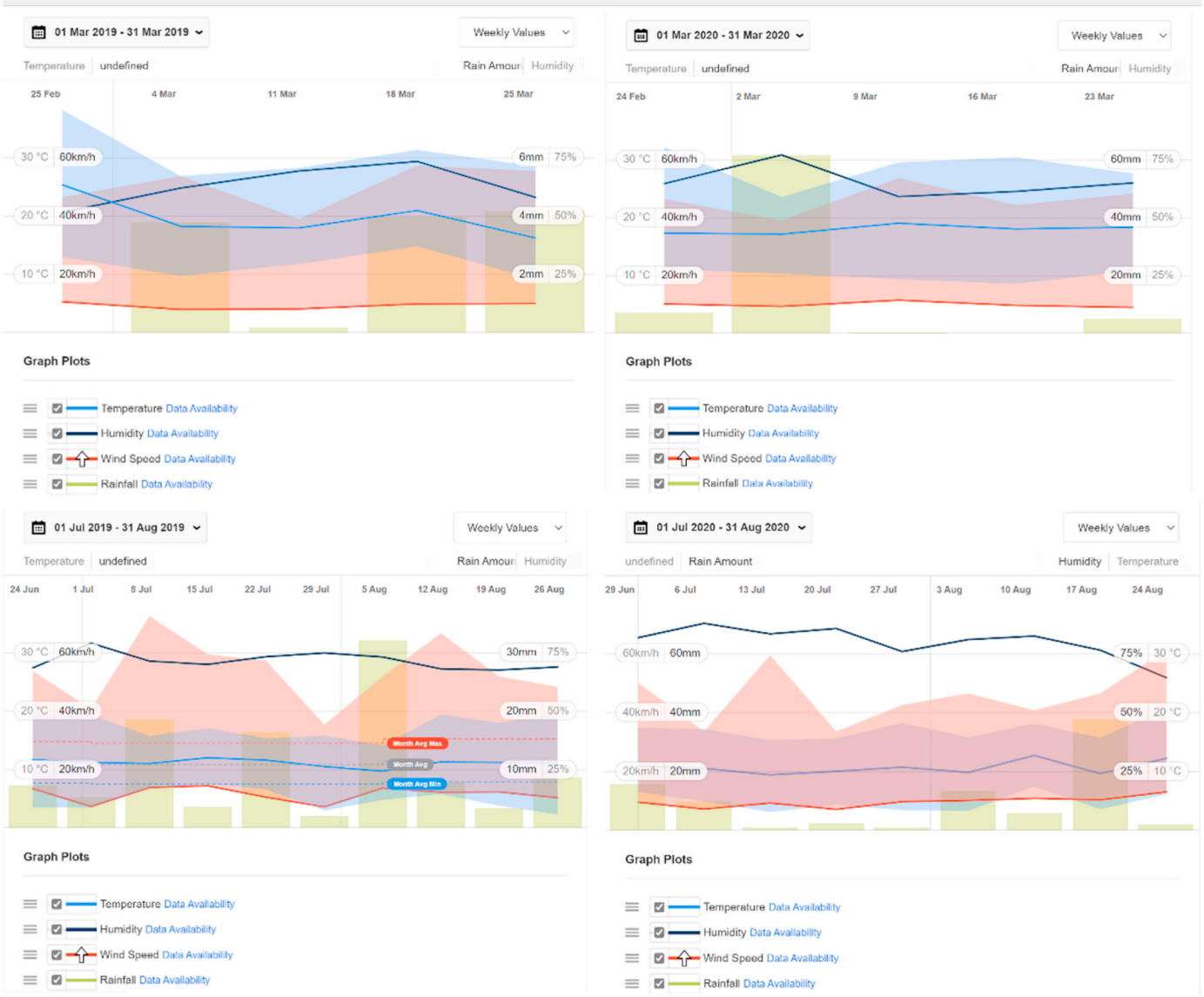


**Fig. 2.** Available weekly meteorological factors at Melbourne Olympic Park weather station during the summertime pre-lockdown (March 2019) and lockdown 2020 (March 2020) (A). Available weekly meteorological factors at Melbourne Olympic Park weather station during the wintertime pre-lockdown (July to August 2019) and lockdown 2020 (July to August 2020) (B) [46].

**Table 1**
Datasets and satellite imagery utilized in this study.

| Factors | Data source and satellite imageries | Satellite imagery products | Factors | Selected bands | Spatial resolution | Temporal resolution | Data info link |
|---|---|---|---|---|---|---|---|
| **Air quality** | Sentinel 5 (TROPOMI multispectral sensor) | NRTI/L3_CO | Near real-time CO | CO_column number_density | | | http://www.tropomi.eu/data-products/carbon-monoxide |
| | | L3_$NO_2$ | Near real-time $NO_2$ | Tropospheric$NO_2$_column_number_density | 3.5 × 7 $km^2$ | Daily | http://www.tropomi.eu/data-products/nitrogen-dioxide |
| | | L3_AER_AI | Near real-time UAI | Absorbing_aerosol_index | | | http://www.tropomi.eu/data-products/uv-aerosol-index |
| | | L3_$SO_2$ | Near real-time $SO_2$ | $SO_2$_columnnumber_density | | | http://www.tropomi.eu/data-products/sulphur-dioxide |
| **SUHI** | MODIS (diurnal and nocturnal) | MOD11A1 | Terra land surface temperature and emissivity daily global 1 km | LST_Day_1 km LST_Night_1 km | 1 km | Daily | [47] |
| | | MYD11A1 | Aqua land surface temperature and emissivity daily global 1 km | | | | |
| **Urban lands (utilized for SUHI calculation)** | Sentinel 1 | S1_GRD | C-band synthetic aperture radar ground range detected and log scaling | HH, HV, VV and VH | 10 m | Daily | [48] |
| | Sentinel 2 | S2 | Multispectral instrument, Level-1C | B4, B3 and B2 | 10 m | 5 days | [49] |
| | NASA SRTM | Elevation | SRTM digital elevation | Elevation | 30 m | _ | [50] |
| **Nighttime lights (*utilized* for energy consumption)** | VIIRS | VCMSLC_FG | Stray light corrected nighttime day/night band composites version 1 | avg_rad | 500 m for composite images | Monthly | [51,52] |
| **Air temperature** | ERA 5-LAND | Monthly averaged by hour of day-ECMWF climate reanalysis | | temperature_2 m | Around 10 km | Average monthly mean based on each hour | [53] |

daily data for the air quality parameters (CO, $NO_2$, UAI, and $SO_2$) were acquired from the Google Earth Engine (GEE) platform and presented in charts and maps.

The LST data provided using MODIS satellite imageries in the GEE platform were used to calculate the SUHI. The MODIS Terra and Aqua satellites provide nighttime and daytime LST maps and charts with the daily temporal and spatial resolution of 1 km. These LST values are prepared with respect to the sensor data acquisition times. MODIS Terra corresponds to ~10:30 a.m. (local solar time) in its descending mode during the day and ~10:30 p.m. in its ascending mode during the night. Furthermore, MODIS Aqua corresponds to ~1:30 p.m. in its ascending mode during the day, and ~1:30 a.m. in its descending mode during the night. In this study, MODIS LST data are mostly used to detect the daily variation of the temperature during the pre-lockdown and lockdown phases. The MODIS LST bands with a spatial resolution of 1 km were utilized to map the average summer and wintertime LST for the City of Melbourne during the lockdown and pre-lockdown phases in 2019 and 2020.

In the SUHI calculation, the urban lands were identified using Sentinel 1 C-band Synthetic Aperture Radar (SAR), Ground Range Detected (GRD), log scaling and Sentinel 2 Multispectral Instrument (MSI), Level-1C and SRTM Digital Elevation Model (DEM). The difference between urban and rural temperatures and the mean rural temperature were calculated, and the SUHI values were identified. The ERA5-Land (monthly averaged by the hour of the day- European Centre for Medium-Range Weather Forecasts (ECMWF) climate reanalysis) and its related 'temperature_2 m' was utilized to calculate the air temperature during the pre-lockdown and lockdown phases (winter and summertime).

Finally, the VIIRS VCMSLC_FG stray light corrected nighttime day/night band composites version 1 and the related band 'avg_rad' were utilized to calculate the lighting energy consumption.

## 3. Methods

The following sections explain the details related to each factor, the corresponding factors, and the related analysis method. A summary of the applied methods is presented in Fig. 3.

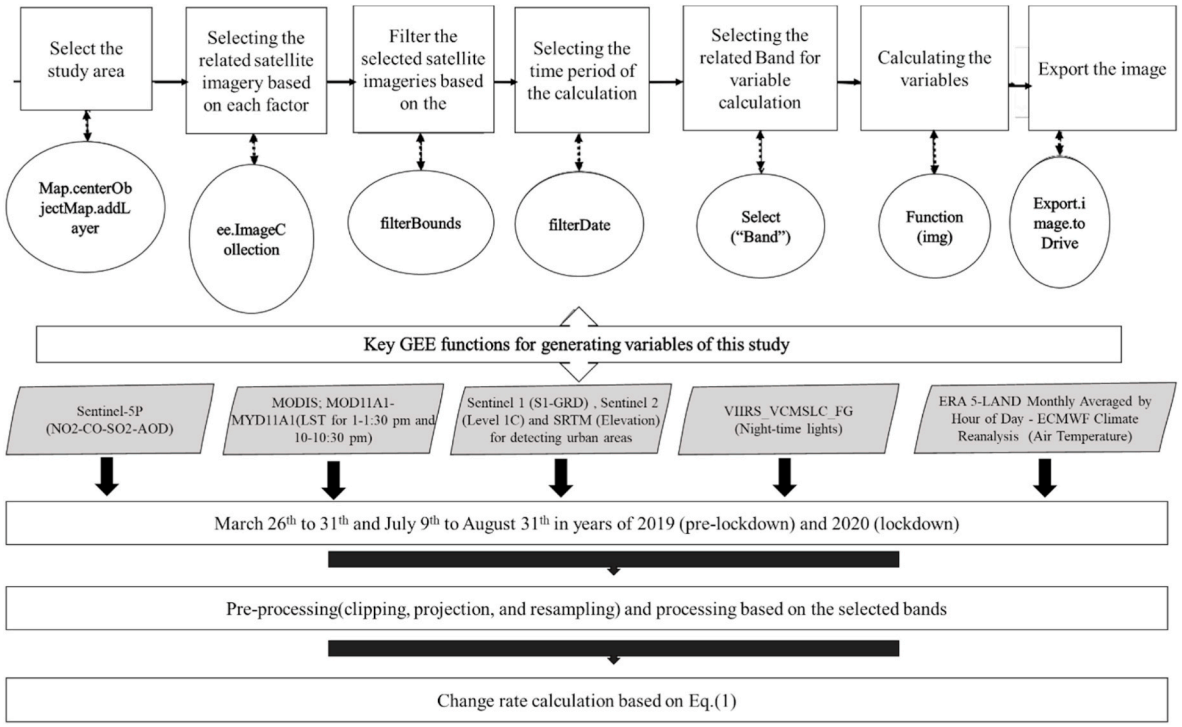


**Fig. 3.** Summary of the research workflow.

### 3.1. Air quality factor calculation

Sentinel-5P TROPOMI was identified as a passive hyperspectral nadir-viewing imager aboard the Sentinel-5 precursor satellite [55].

Since July 2018, TROPOMI has provided calibrated and near real-time data (from the nadir-viewing spectrometer), which could be used to assess air quality, including formaldehyde, aerosol, and CO, $NO_2$, and $SO_2$ [56]. Griffin et al. [57] and Lorente et al. [58] showed that the TROPOMI measurement is relatively well connected with the actual ground measurements and available crowd-sourced data n air quality parameters. The TROPOMI products used were L3 Near Real Time (NRTI) version products with a spatial resolution of $3.5 \times 7$ km$^2$ [54,59]. Sentinel-5P was located at an altitude of 817 km in an ascending mode with an equator crossing time at 13:30 p.m. (local time) with daily global coverage. Fig. 3 shows the key steps to generate maps and charts for air quality factors.

After generating maps and diagrams for each air quality factor, the change rate (concentration) was also calculated to present the percentage of the change in air quality factors in the City of Melbourne during the lockdown and pre-lockdown periods of the summer and winter months in 2019 and 2020. The variation change rate in the air quality factors between March 26–31 (summer) and June to August (winter) of 2019 and 2020 was examined using Eq. (1), as follows:

$$\text{Change rate} = \frac{\text{Factor } 2020 - \text{ Factor } 2019}{\text{Factor } 2019} \times 100. \quad (1)$$

The average monthly change rate values of the air quality factors were compared because the values of the air quality factors were available on different days in the summer and winter seasons during the pre-lockdown and lockdown periods. The trimmed mean function was used after sorting the values from small to large to remove the effect of outliers in the calculation process of the average available values of the air quality factors, as follows:

$$\text{Trimmed Mean} = \frac{\sum_{(N\times P)+1}^{N\times(1-P)} Xi}{N \times (1-2p)}. \quad (2)$$

where $N$ is the number of observations, $P$ is the trimming per cent observations from the dataset, and Xi is the value of the related factor.

### 3.2. LST and SUHI calculation

The daily LST values during nighttime and daytime were provided by the MODIS Terra (MOD11A1) MV6 and Aqua (MYD11A1) products in a $1200 \times 1200$ km grid [60]. Furthermore, the temperature values were provided by the MOD11_L2 swath product. The temperature pixel value was the average of all qualifying observations when the latitude of the study area was above 30°, given that a few LST pixels could provide multiple observations when the sky is clear. In addition, the quality indicator layers were MODIS bands 31 and 32 and six observation layers [47]. Furthermore, Wang, et al. [61] have validated MODIS LST products. In its comparison of the LST products (SUHI maps) with air quality factors and lighting energy consumption, this study only focused on MODIS Terra nighttime and MODIS aqua daytime.

The main steps for calculating the MODIS LST were similar to those shown in Fig. 3. After providing the LST products with MODIS Aqua and Terra, the urban areas were defined to generate SUHI products. The urban land mapping was conducted using the proposed method of Sun et al. [62]. The authors mainly used the ascending/descending orbits of Sentinel-1A SAR data and Sentinel-2 MSI Level 1C in the GEE platform. The yearly Normalized Difference Vegetation Index (NDVI) maximum and modified Mean Normalized Difference Water Index (MNDWI) mean composite was generated from Sentinel-2 imagery. Indeed, the time series of the NDVI and the MNDWI is derived from a time series of Sentinel-2 images. Multi-temporal NDVI indices were utilized to generate a maximum composite NDVI, and after that, a mean reducer was applied to the time series of MNDWI to generate the yearly average value of MNDWI (MNDWI_mean).

Furthermore, the DEM is used for generating mountain masks (slope image). Masks of vegetation, water and mountain pixels were obtained by applying thresholds for NDVI_max, MNDWI_mean and slope image, respectively. In the next step, the potential urban lands from Sentinel-1A were utilized to extract the target urban land (TUL) through a threshold

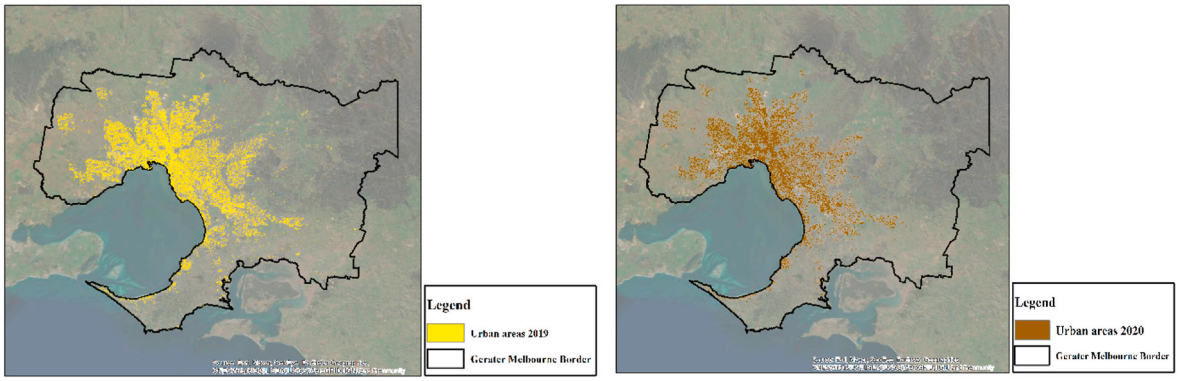


**Fig. 4.** Urban lands of Greater Melbourne in 2019 and 2020.

segmentation method. A final urban land was derived by applying a three-by-three majority filter on the target urban land after masking water, vegetation and mountains regions.

The proposed methodology of Sun et al. [62] was implemented in the GEE platform in Greater Melbourne (link is attached) to identify the urban lands. Fig. 4 shows the generated urban land areas in 2019 and 2020.

In the next step, SUHI was measured based on Eq. (3), which was reviewed by Stewart [63] and Yao et al. [64] using ArcGIS pro software [65] to account for the difference of LST between urban and rural areas. The average LST of the rural areas was calculated and subtracted from the LST of the urban areas considering all pixels.

$$\text{SUHI} = \text{LST urban} - \text{LST rural}. \quad (3)$$

### 3.3. Air temperature calculation

The ERA5-Land was used to calculate the mean value of air temperature in winter (July and August) and summer (March) for each month and the total average air temperature for the available dates during the winter and summer seasons during the lockdown and pre-lockdown periods (2019 and 2020). The 'temperature_2 m'selected as a primary product of ERA5-Land, explains the air temperature at 2 m (in Kelvin) above the land's surface, sea, or in-land waters [53].

Similar steps for MODIS LST and air quality factor analysis (Fig. 3) were considered to assess and calculate the air temperature values. The band 'temperature_2 m' was selected, and the calculated air temperature in Kelvin was converted into Centigrade in the last step.

### 3.4. Lighting energy consumption

The energy consumption was calculated based on the monthly average radiance composite images using nighttime data from the VIIRS Day/Night Band (DNB). The version 1 VIIRS-DNB monthly images were obtained from the National Oceanic and Atmospheric Administration (NOAA) National Centers for Environmental Information (NCEI). Furthermore, each DNB pixel contained information on the mean detected radiance (expressed in nanowatts/cm2/sr units) [66].

Many previous studies have demonstrated that the brightness of Night Time Light (NTL) derived from satellite images is a good proxy for identifying urban agglomerations and human settlements [67,68]. In addition, the alteration of the brightness of NTL most likely reflects the change in urban development. However, studies on the application of NTL imageries on energy and lighting energy consumption, especially in Australia, are still limited.

The monthly composites of the VIIRS NTL image during the pre-lockdown and lockdown summer and winter seasons were used and analyzed in the GEE platform to investigate the lighting energy consumption. During the NTL image processing, pixels identified as sensor calibration noise and with negative values and those with small radiance values were removed. The pixels with small radiance values were removed to reduce the impact of land surface albedo and vegetation phenology on the NTL pixels. Therefore, similar to Falchetta and Noussan [69] study, the pixel values below 0.25 were removed and set to zero.

The unit of 'avg_rad' band of the VIIRS imageries (nanowatts/cm2/sr) is not useful for comparing the light values for different city areas. Therefore, Eq. (4) was used for each pixel based on Zhu and Blackborow [70] and the PNGK [71] document:

$$1(\text{nanowatts} / \text{cm2} / \text{sr}) = 0.322 \ \text{W}. \quad (4)$$

Each pixel's width value (15 arc seconds) at the equator was changed to an arc second of longitude, which is approximately equal to an arc second of latitude (approximately 30 m). In the next step, the steradian SR of each pixel, which is the corresponding SI unit for measuring solid angles, was multiplied by $(1/2\pi)$ to generate a pixel that was reflected on the flat surface. Finally, the nanowatts were converted into watts, and the pixel value was multiplied by 0.322 to obtain the sum of all pixel values within the selected city boundary.

## 4. Results and discussion

### 4.1. Air quality factors

The following sections present the statistical trends of the air quality factors and the related maps of their mean values during the summer and wintertime in the City of Melbourne during the pre-lockdown and lockdown phases. Furthermore, the results of air quality factors are compared with those of the other studies.

#### 4.1.1. $NO_2$

$NO_2$ is released into the atmosphere due to anthropogenic activities, such as fossil fuel combustion and soil microbiological processes, wildfires, and lightning.

Fig. 5 depicts that the highest value of the available $NO_2$ during pre-lockdown (0.313 mol/m$^2$) was higher than the highest available $NO_2$ value during the lockdown (0.128 mol/m$^2$) in March. In addition, the minimum values of $NO_2$ during lockdown and pre-lockdown are 0.070 and 0.078 mol/m$^2$, respectively, and close to each other. The comparison between the mean value of $NO_2$ during the lockdown and pre-lockdown summertime showed that the mean $NO_2$ value decreased from 0.165 mol/m$^2$ from the pre-lockdown (March 2019) phase to 0.082 mol/m$^2$ during the lockdown phase (March 2020). The higher amount of $NO_2$ during the summer of 2019 aligns with the findings of Ryan et al. [72]. The authors suggested that temperature is one of the most important meteorological factors controlling pollutant concentrations. The high temperature observed during March 2019 compared with March 2020 [73,74] indicates that higher temperatures are

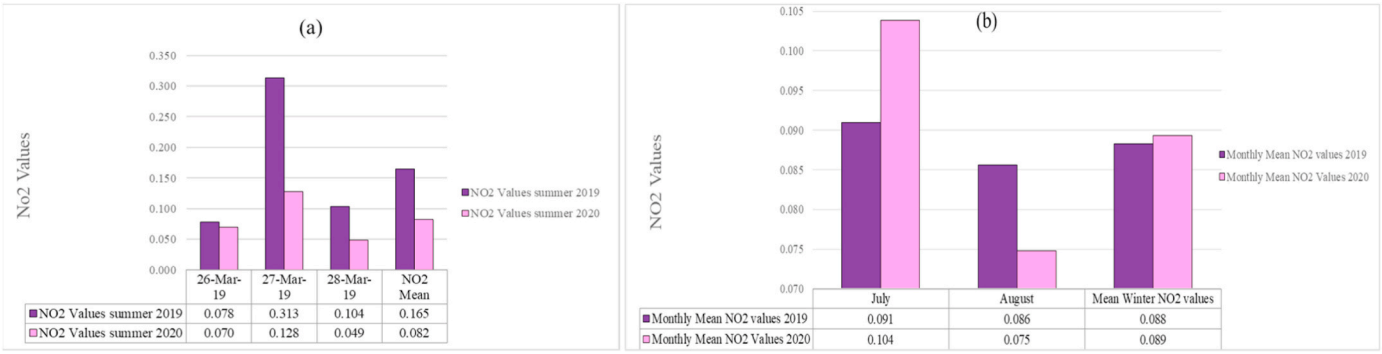


**Fig. 5.** Available $NO_2$ values (mol/$m^2$) for summertime (March) (a) and the monthly mean $NO_2$ values (b) during pre-lockdown (2019) and lockdown (2020) at 1:00–1:30 p.m.

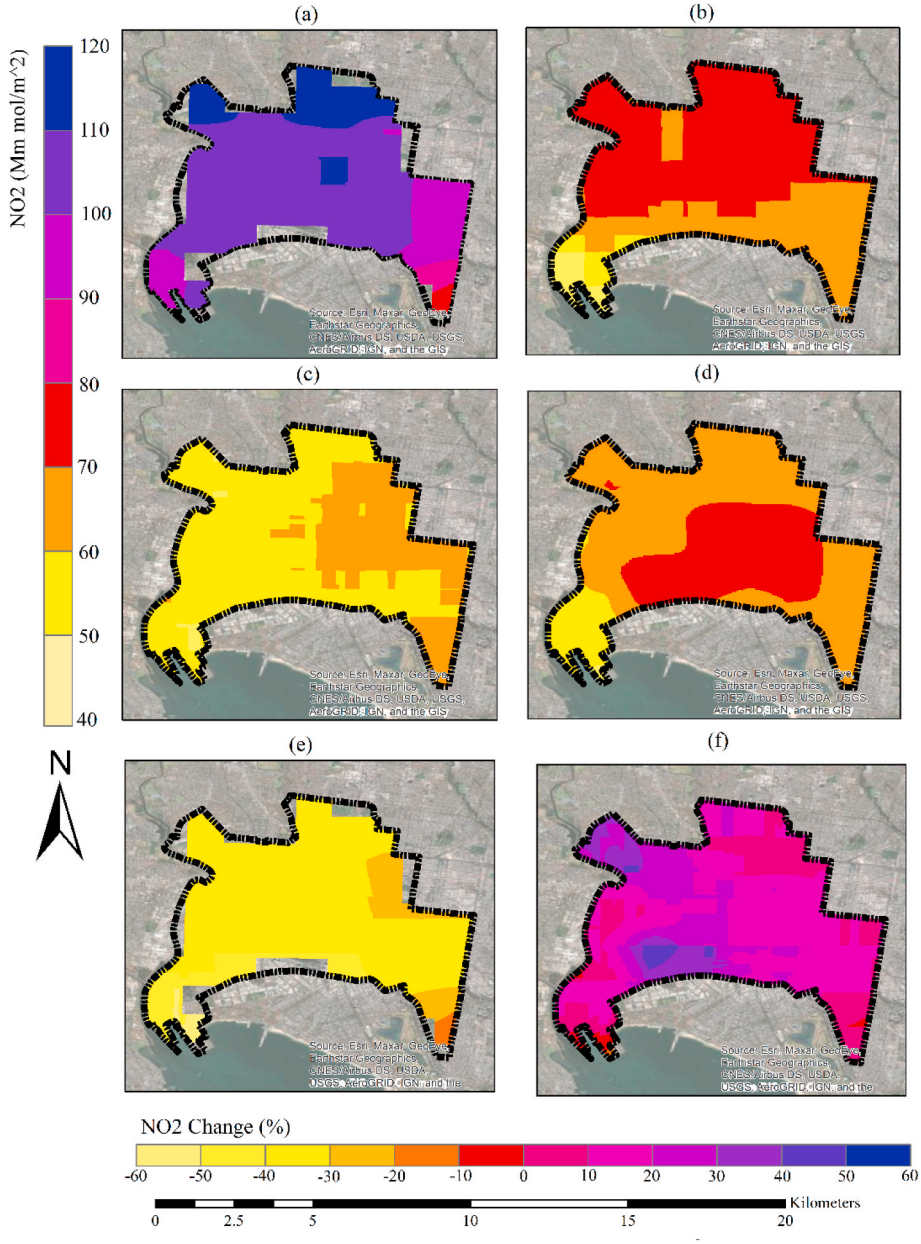


**Fig. 6.** Spatiotemporal distribution of mean $NO_2$ (Mm mol/$m^2$) over the City of Melbourne: (a) March 2019 (pre-lockdown), (b) March 2020 (lockdown), (c) winter 2019 (pre-lockdown), (d) winter 2020 (lockdown), (e) mean $NO_2$ change rate (%) between pre-lockdown and lockdown during summer and (f) mean $NO_2$ change rate (%) between pre-lockdown and lockdown during winter.

responsible for the higher number of $NO_2$ concentrations during summer (March) 2019. The reduction in mean $NO_2$ value during summer can be related to the complex photochemical reactions, which occur under the influence of solar radiation [75]. The decrease in the transportation sector emissions was primarily affecting the $NO_2$ reduction.

By contrast, the mean $NO_2$ values during the wintertime lockdown and pre-lockdown phases slightly increased from 0.088 mol/$m^2$ to 0.089 mol/$m^2$. Furthermore, while the mean $NO_2$ values increased from 0.091 mol/$m^2$ to 0.104 mol/$m^2$ during the month of July in winter, the $NO_2$ values reduced in August. During winter, the lockdown started on July 9, and the $NO_2$ values were higher than those of the previous year (pre-lockdown). Notably, during winter, the $NO_2$ would be in the air for longer than during summer, resulting in air pollution. Furthermore, the number of people that stayed home increased during the lockdown.

Consequently, energy usage for heating also increased. Another reason for the increase in the $NO_2$ values during lockdown could be temperature inversion. During inversion, the dense layer of cold air is trapped under the warm air layer, which keeps pollutants in the cold air near the ground.

Figs. 5 and 6 show that $NO_2$ covered most areas within the range of 100–110 Mm mol/$m^2$ during the pre-lockdown period in March. However, during the lockdown, the values were reduced to 30 Mm mol/$m^2$. Furthermore, near the Fishermen's Bend shipping and cargo precinct, the southwestern areas experienced the most significant drop in $NO_2$ values due to traffic emission reduction, which aligns with Talbot et al. [76] and Patel et al. [77].

During the winter months of July and August, most areas were covered by $NO_2$ with values of 50–60 Mm mol/$m^2$, lower than during the summer's pre-lockdown. During the lockdown, the most dominant $NO_2$ values were within the range of 60–70 Mm mol/$m^2$, which negligibly increased (10 Mm mol/$m^2$) compared with the pre-lockdown phase. Furthermore, the CBD areas during the lockdown and pre-lockdown had higher $NO_2$ values than the other locations in the City of Melbourne. Some main reasons for the increase of $NO_2$ during the lockdown in the CBD could be related to temperature inversion and the prevalence of high-rise buildings, resulting in the trapping of $NO_2$ in those areas. The $NO_2$ geospatial status in Melbourne CBD can be related to Talbot and Lehn [78]. The authors mentioned that operating diesel-fueled bus services for the use of essential workers represented a major contribution to the $NO_2$ concentrations, especially along busy urban canyons.

In summer, the $NO_2$ values during lockdown from 2019 to 2020 decreased (40%–50%). However, the $NO_2$ values in most areas in winter increased during lockdown from 2019 to 2020. Notably, the food industry precinct on the western side of the suburb of Kensington and the harbour suburb of Docklands increased in $NO_2$ values by more than 40% during the lockdown.

#### 4.1.2. CO

CO is considered a major atmospheric pollutant in certain urban areas. CO contains the combustion of fossil fuels, biomass burning, and atmospheric oxidation of methane and other hydrocarbons [79].

Fig. 7 indicates that the highest value of CO during lockdown (0.023 mol/$m^2$) in March was higher than the highest CO value during pre-lockdown (0.019 mol/$m^2$). In addition, the minimum CO values during lockdown (0.021 mol/$m^2$) were higher than the minimum CO value during pre-lockdown (0.017 mol/$m^2$). Fig. 7 shows that the mean value of CO increased from 0.018 mol/$m^2$ to 0.022 mol/$m^2$ during March for the pre-lockdown (2019) and lockdown (2020) phases. Similar to summertime (March), the mean CO values slightly increased from 0.021 mol/$m^2$ to 0.022 mol/$m^2$ from pre-lockdown (2019) to lockdown (2020) during winter. The increase in CO values in July and August was also negligible.

The CO alterations were insignificant despite their increase, especially in summertime (approximately 23%). As discussed in Hernández-Paniagua et al. [80], this finding could be related to the burning of natural gas during the lockdown when people stayed at home. Furthermore, a slight increase in CO during lockdown was found by Tello-Leal and Macías-Hernández [81] in their study in Mexico. In the aforementioned study, the constant decrease in temperature (similar to the Melbourne March 2019 and March 2020 temperature comparison) resulted in a slight increase in CO concentration levels. This could also be related to the presence of rainfall. In the City of Melbourne, the average of rainfall in the targeted weather station (Melbourne Olympic Park) during March 2020 was lower, resulting in a higher amount of CO during the summer lockdown (2020).

An increase in CO values during lockdown was detected by Zhou et al. [82] in south China due to fire emissions; however, the results of the current study contrast with those findings. Based on the City of Melbourne emission reduction document [83], the number of emissions will reduce according to the emission reduction pathway. The CO values increased during the lockdown while emissions were reducing, mainly affected by the meteorological parameters, such as wind and temperature.

Fig. 8 shows the slight difference between the CO values in the different areas during the pre-lockdown phase. Most southeastern areas had mean CO values between 17 Mm mol/$m^2$ and 18 Mm mol/$m^2$. However, the mean CO values of these areas during the lockdown increased to the range of 20–21 Mm mol/$m^2$. The highest CO values during the pre-lockdown phase in March were spatially distributed in the southwest near the Port Melbourne neighbourhood and Fishermen's Bend area. However, the spatial distribution of the highest CO values ranging from 22 Mm mol/$m^2$ to 23 Mm mol/$m^2$ covered the city's northern parts during the lockdown, where most parks and grasslands are located. In addition, the LST values of the northern parts of the City of Melbourne (for instance, the Flemington Racecourse horse track)

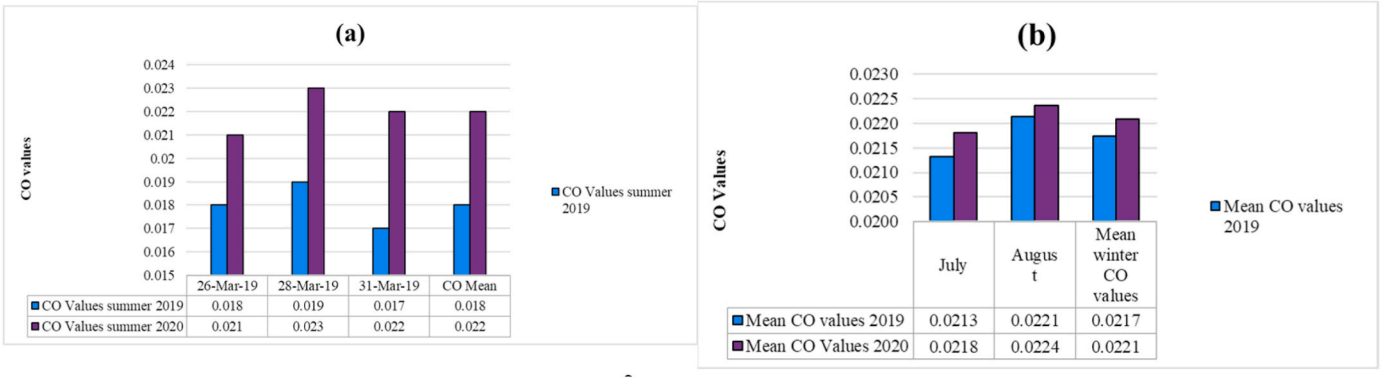


**Fig. 7.** Available CO values (mol/$m^2$) for summertime (March) (a) and the monthly mean CO values (b) during the pre-lockdown (2019) and lockdown (2020) at 1:00–1:30 p.m.

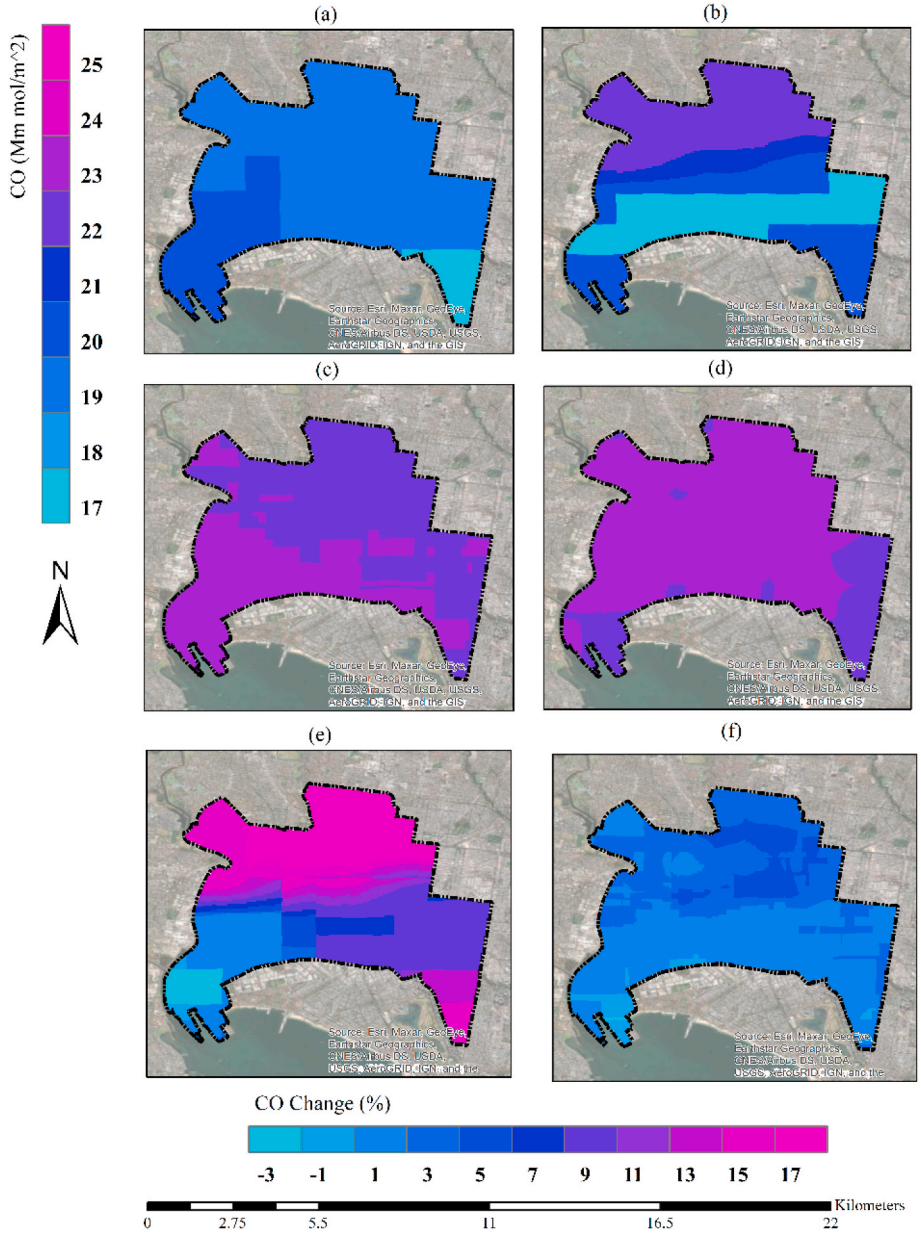


**Fig. 8.** Spatiotemporal distribution of mean CO (Mm mol/m$^2$) over the City of Melbourne: (a) March 2019 (pre-lockdown), (b) March 2020 (lockdown), (c) winter 2019 (pre-lockdown), (d) winter 2020 (lockdown), (e) mean CO change rate (%) between pre-lockdown and lockdown during summer and (f) mean CO change rate (%) between pre-lockdown and lockdown during winter.

during lockdown 2020 were 3 °C lower compared with the March pre-lockdown phase (2019). As previously mentioned, the lower temperature (LST) values resulted in higher CO values during the summer lockdown in 2020.

During the lockdown, the lowest range of CO values (17–18 Mm mol/m$^2$) mostly covered the southern areas of the City of Melbourne, where high-rise buildings, Docklands harbour and the Yarra River are located.

Fig. 8 also reveals that the CO values increased during winter (pre-lockdown and lockdown) compared summertime. The increasing CO emissions could be attributed to vehicle cold starts and reduced fuel combustion efficiency [84]. In addition, people are more likely to use heaters in winter, especially at home during the lockdown, thereby increasing the CO values in winter.

During the winter lockdown, more areas were covered by the CO values within the range of 23–24 Mm mol/m$^2$. The difference between mean CO values during the winter pre-lockdown and winter lockdown phases was negligible at only 1 Mm mol/m$^2$.

The highest positive change rate (17%) during summer was detected in the southeast and northern areas, where more green areas are located. However, the positive CO change rate during winter had a lower percentage (3%–5%) in the northern areas. The temperature (LST) in the northern areas during winter lockdown (2020) is 2 °C higher, whilst the CO values are slightly higher (0.19) Mm mol/m$^2$ in those areas. The relationship between temperature (LST) and CO values in the northern areas contrasts with the summertime.

One main reason for the high concentration of CO in green areas could be related to the wind direction. Amorim et al. [85] indicated that the CO emission level at the pedestrian level increased when the incoming wind direction was approximately 45° due to the trees' impact on the exchange rates with the air above the roof level.

#### 4.1.3. $SO_2$

$SO_2$ enters the Earth's atmosphere naturally and by anthropogenic

processes. $SO_2$ mainly has an anthropogenic origin, and 30% of emitted $SO_2$ comes from natural sources. The significant adverse effect of $SO_2$ is related to the formation of sulphate aerosols. Fig. 9 shows the comparison between the $SO_2$ values during the pre-lockdown and lockdown phases indicates that the mean $SO_2$ (330 μm mol/$m^2$) value during the lockdown was slightly higher compared with during the pre-lockdown (−330 μm mol/$m^2$). The negative $SO_2$ values are artefacts of the retrieval process and are normally connected to the $SO_2$ retrievals over highly reflective surfaces. While negative values are not actual values, the measurements are still valid and should not be discarded during the pre-lockdown in the summertime (March 2019). Meanwhile, the mean $SO_2$ values decreased from pre-lockdown to lockdown (from 570 μm mol/$m^2$ to 460 μm mol/$m^2$) during winter (except in July, where the available $SO_2$ in 2019 was less).

The reduction in $SO_2$ during winter is mostly associated with the reduction in industrial activities and vehicle traffic. In addition, the amount of incineration and commercial ship activity significantly reduced due to the lockdown, thereby contributing to $SO_2$ emissions. The two possible reasons for the higher $SO_2$ values during the lockdown than pre-lockdown are as follows. Firstly, implementing government lockdown restrictions required two to three days of lag time. Secondly, some government offices were still open during the lockdown, and some essential workers were still commuting to the city.

Fig. 10 shows that the highest values of $SO_2$ (410 μm mol/$m^2$) and the dominant range (475–675 μm mol/$m^2$) during pre-lockdown were spatially distributed on the west side of the city, near Fishermen's Bend and the loading docks. These areas had higher $SO_2$ values mainly because of the heavy vehicle traffic. During the lockdown, the highest $SO_2$ values slightly increased (310 μm mol/$m^2$). The maximum $SO_2$ values during the lockdown were spatially distributed in the southwest of the city, where most high-rise buildings are located. The higher $SO_2$ values during the lockdown in these areas are similar to the findings of Zheng et al. [86], who mentioned that the $SO_2$ shows a strong positive correlation with road density and LST. Furthermore, in this case, it should be acknowledged that $SO_2$ can easily be produced under high temperature and humidity conditions, as reflected in the meteorological parameters of Melbourne during the pre-lockdown and lockdown summertime (Fig. 2).

During winter and pre-lockdown, the highest $SO_2$ values (ranging from 675 μm mol/$m^2$ to 1060 μm mol/$m^2$) were mostly spatially distributed in the southeast, where high-rise buildings are located. By contrast, the highest $SO_2$ values ranging from 475 μm mol/$m^2$ to 675 μm mol/$m^2$ during lockdown were spatially distributed in the southwest around the loading dock areas. Furthermore, more areas were covered with a higher range of $SO_2$ values during the lockdown.

The change rate values show that the $SO_2$ reduction during summer was evident primarily in the areas near the Fishermen's Bend, where the vehicle and truck traffic were reduced due to the lockdown. Meanwhile, the $SO_2$ values increased during the lockdown in areas with high-rise buildings due to the heating and cooling system usage. The lower levels of the buildings demonstrated a much higher pollution rate than the upper floors, especially in areas with weak winds. The $SO_2$ distribution and other air pollution factors in an urban environment depend on the architectural layout, the proximity to green space, and the wide spaces between the buildings that promote better circulation of the air pollutant dispersion [87]. The proximity of neighbourhoods to industrial land uses is another factor that affects the spatial distribution of $SO_2$ change rate during winter. During the winter lockdown, the southeastern suburbs were affected mainly by the Southbank industrial areas. Abdullahi et al. [88] also mentioned other factors contributing to this, such as the residents' income and their ability to purchase cooling and heating systems.

#### 4.1.4. UAI

UAI indicates the presence of elevated absorbing aerosols in the Earth's atmosphere. The positive values of the Aerosol Index represent the absorbing aerosols (dust and smoke), whilst the small or negative values denote the non-absorbing aerosols and clouds.

The aerosol types primarily seen in the UAI are desert dust and biomass-burning aerosols. The Aerosol Index calculation is based on the wavelength-dependent changes in Rayleigh scattering in the UV spectral range, where ozone absorption is very small [89].

Aerosols are particles formed by solid or liquid particles dispersed and suspended in the air. Furthermore, aerosols contain soil particles, industrial dust particles, particulates emitted by vehicles, microorganisms, plant spore powders, and other components.

Kumar [90] suggested that COVID-19 might transmit over long distances in open spaces through aerosols. COVID-19 could be dissolved with the aerosol and become bio-aerosols, which range from 1.0 μm to 5.0 μm and can travel hundreds of meters or more.

Fig. 11 indicates that in March, the highest absolute value of available aerosols during pre-lockdown (|2.93|) was higher than the highest absolute available aerosol value during lockdown (|1.421|). Furthermore, the minimum absolute value of aerosols during the pre-lockdown (|0.453|) was lower than the minimum absolute value during the lockdown (|0.814|). The comparison between the absolute mean value of aerosols during the lockdown and pre-lockdown (summer) showed that the mean absolute aerosol value increased by approximately 0.009.

Similar to summertime (March), the mean absolute value of aerosols during winter slightly increased from |1.073| to |1.274|. Furthermore, the highest increase in the absolute mean value of aerosols was in July, with a change rate of 23.78%.

The number of aerosols increased significantly during the summer lockdown than during the winter lockdown. During the winter lockdown

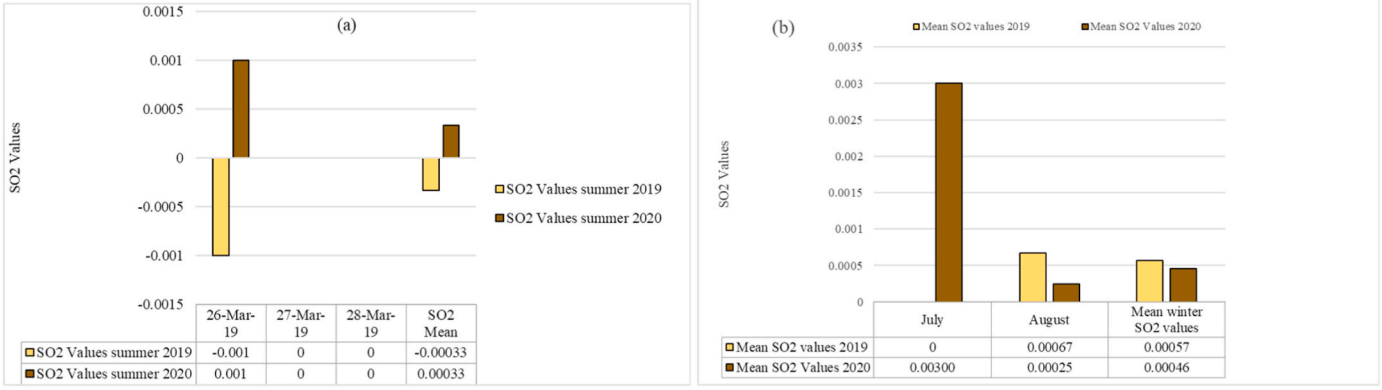


**Fig. 9.** Available $SO_2$ values (mol/$m^2$) for summertime (March) (a) and the monthly mean $SO_2$ values (b) during the pre-lockdown (2019) and lockdown (2020) at 1:00–1:30 p.m.

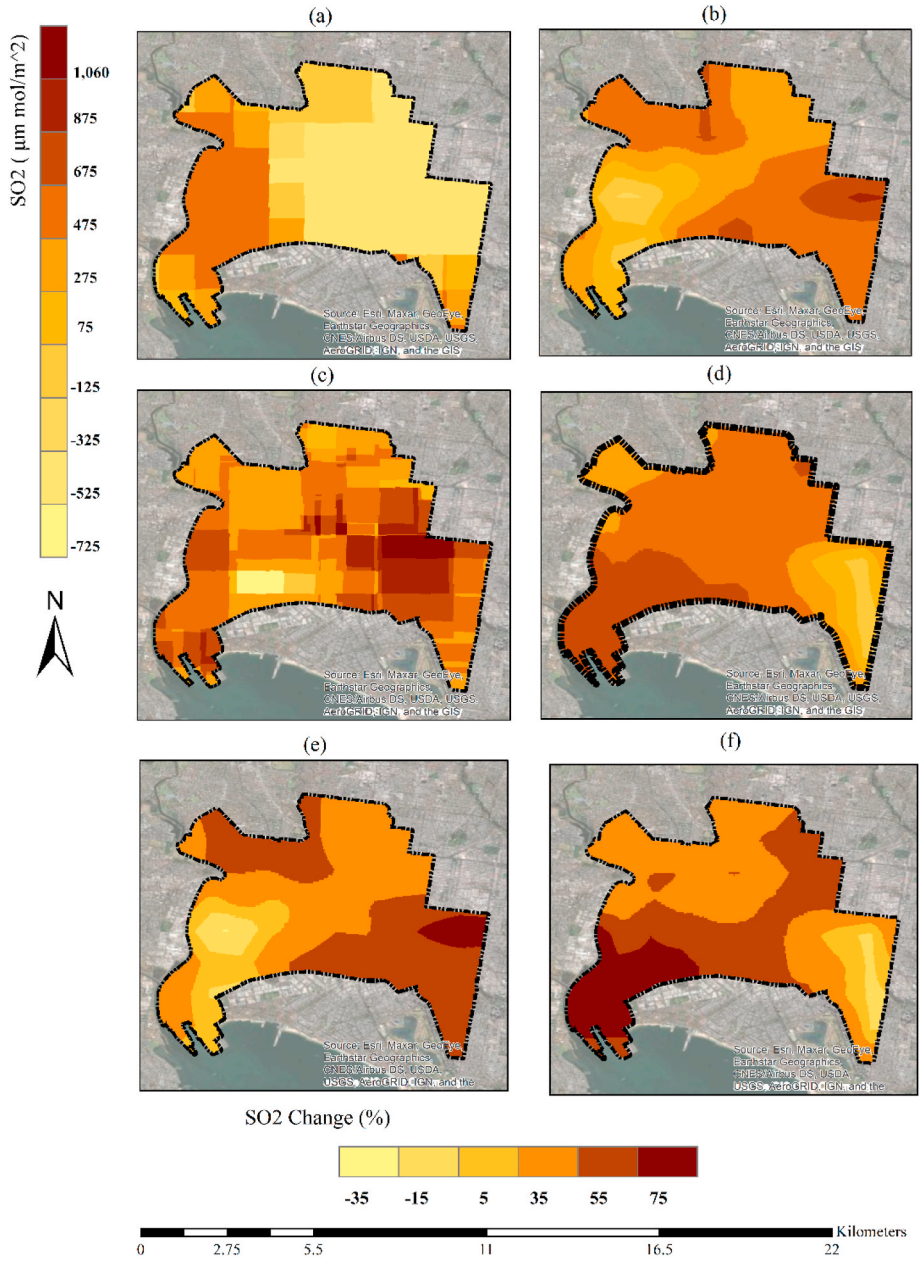


**Fig. 10.** Spatiotemporal distribution of the mean $SO_2$ (µm mol/$m^2$) over the City of Melbourne: (a) March 2019 (pre-lockdown), (b) March 2020 (lockdown), (c) winter 2019 (pre-lockdown), (d) winter 2020 (lockdown), (e) mean $SO_2$ change rate (%) between pre-lockdown and lockdown during summer and (f) mean $SO_2$ change rate (%) between pre-lockdown and lockdown during winter.


| | 26-Mar-19 | 27-Mar-19 | 28-Mar-19 | 29-Mar-19 | 30-Mar-19 | 31-Mar-19 | AI Mean |
|---|---|---|---|---|---|---|---|
| AI Values summer 2019 | -0.826 | -0.610 | -0.691 | -0.453 | -2.933 | -1.161 | -1.112 |
| AI Values summer 2020 | -1.087 | -1.048 | -1.042 | -0.814 | -1.315 | -1.421 | -1.121 |

| | July | August | Mean winter AI values |
|---|---|---|---|
| Mean AI values 2019 | -1.083 | -1.063 | -1.073 |
| Mean AI Values 2020 | -1.340 | -1.208 | -1.274 |

**Fig. 11.** Available UAI values for summertime (March) (a) and monthly mean UAI values (b) during the pre-lockdown (2019) and lockdown (2020) at 1:00–1:30 p.m.

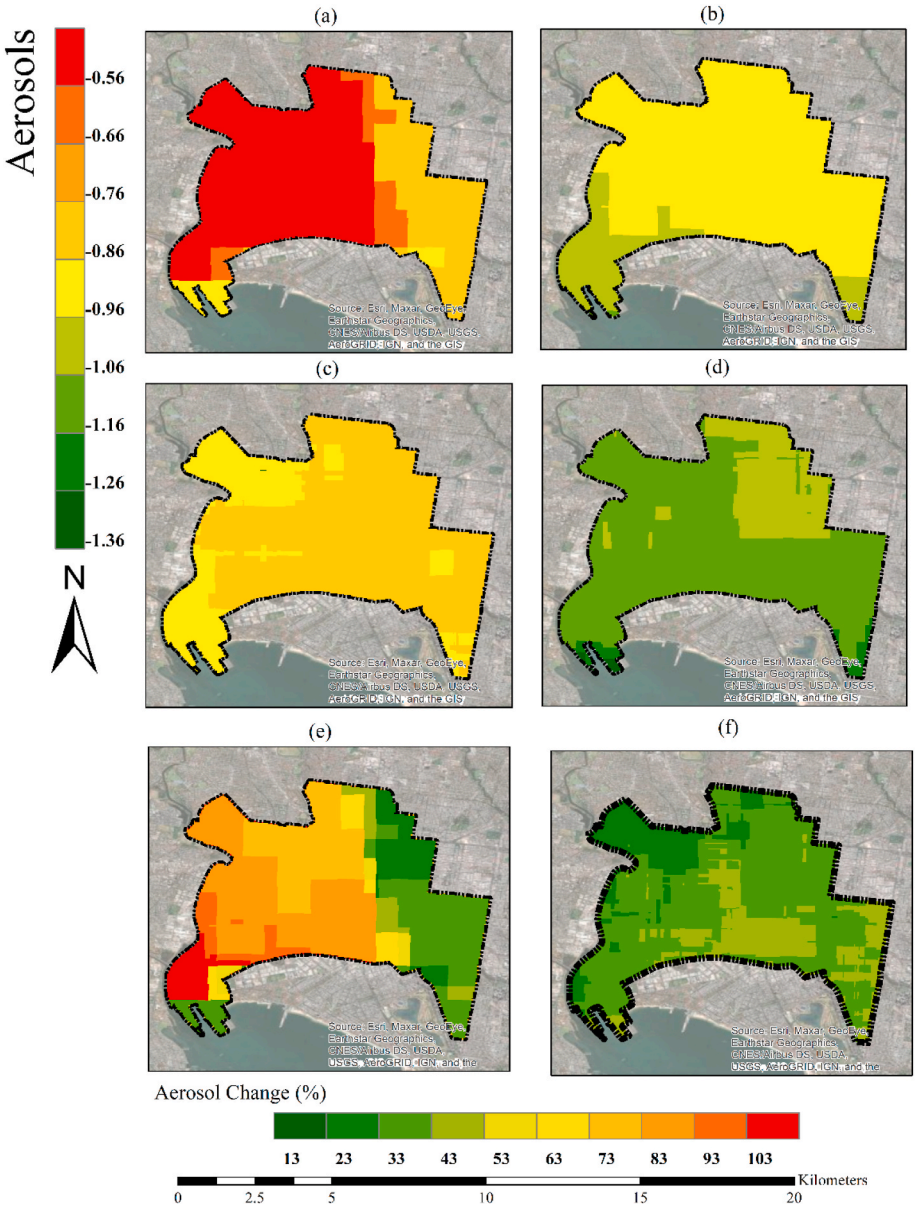


**Fig. 12.** Spatiotemporal distribution of the mean UAI over the City of Melbourne: (a) March 2019 (pre-lockdown), (b) March 2020 (lockdown), (c) winter 2019 (pre-lockdown), (d) winter 2020 (lockdown), (e) mean UAI change rate (%) between pre-lockdown and lockdown during summer and (f) mean UAI change rate (%) between pre-lockdown and lockdown during winter.

(especially August), the aerosol values increased due to the higher number of bushfires affecting Greater Melbourne, thereby adjusting the volume of burned biomass in the air. In addition, the harvest time in Melbourne and Victoria did not overlap with the lockdown phases (summer and winter). Thus, the number of aerosols did not increase due to harvesting and crop residue burning.

Fig. 12 shows that most areas during the March pre-lockdown were covered by aerosol absolute values lower than |0.56|. However, the most dominant absolute values of aerosols during the lockdown were within the range of (|0.96|–|0.86|), representing an increase in the aerosols' absolute values. The results are similar to the study of Chi et al. [91]. The authors mentioned that the increased values of $PM_{2.5}$ as one of the UAI pollution factors could be related to the mass demonstrations and protests that occurred in response to the lockdown and government policies.

The southwestern areas have higher absolute values during the lockdown. Furthermore, the aerosol change rate is higher in areas near Docklands harbour than in the suburb of Port Melbourne. The increasing absolute values of aerosols are related to the land use types in those areas, mainly industrial. According to WMO [92], urban/industrial emissions are primary sources of aerosols.

Most areas during the pre-lockdown wintertime were covered by aerosol values ranging from |0.76| to |0.86|), which are higher than those during the pre-lockdown summertime. During the winter lockdown, the most dominant absolute aerosol values were within the range of |1.06|–|1.16|, which negligibly increased compared with the summertime lockdown. The southwestern areas have higher aerosol values than the other locations. The higher aerosol values in these areas (mainly construction areas) were also reflected in Xie and Sun [93], where a positive correlation was detected between Normalized Difference Built-up Index (NDBI) and Aerosol Index.

The comparison between the change rate of aerosol absolute values during the summer and winter shows that the spatial alteration of aerosol is slightly more important during summer, especially in areas covered mostly with impervious surfaces (e.g. the west side of the City of Melbourne). According to Oke [94], warmer urban surfaces with a higher LST could emit a larger upward longwave radiation, promoting

the heating of the atmosphere through the absorption of the aerosols and the subsequent re-emission of the longwave radiation. As such, the UHI-related warm temperature promoted the turbulent dispersion of aerosol particles in the urban areas [95] that can be seen in the south and southwestern parts of the City of Melbourne.

This situation is also comparable with Talbot et al. [76], who mentioned that domestic heating is the main reason for the Aerosol Index increment. Talbot et al. [76] also explained that the $PM_{10}$ and Aerosol Index concentrations are affected by sea salt near coasts, dust and resuspended road dust, and wood smoke from wood burning for fuel, which can be seen in the southwestern areas of the City of Melbourne in Fishermen's Bend and Docklands, which are near the coast. The Fishermen's Bend area has a few timber suppliers and warehouses that could cause wood dust that would affect the UAI concentration in that area.

Similar to the other air quality factors, the UAI is affected by meteorological parameters, such as higher winds, which can bring high sea salt concentrations, thus elevating UAI mass across coastal areas [96]. This situation is more evident during the summer, with the UAI index being slightly higher during the lockdown summertime when the average wind speed was slightly higher (10.1 km/h) compared with the pre-lockdown summer (9.4 km/h) [46]. During the winter, lower wind speeds can help elevate the UAI concentrations due to home heating sources, which appears to be the case for the Melbourne CBD area where high-rise residential buildings are located. Household emissions increased during the lockdown because of higher home occupancy compared with during the pre-lockdown phase.

Fig. 13 shows an overview of the change rate between the different air quality factors. Among the various factors, the highest percentage of positive change rates from pre-lockdown to lockdown belonged to aerosol and CO in the summertime, whereas the lowest percentage belonged to $SO_2$ and $NO_2$.

### 4.2. SUHI

The SUHI alteration during the available days of the March and winter months was investigated using MODIS Aqua and Terra's daytime and nighttime LST bands, with the City of Melbourne as the research area and the mean LST values collected from rural areas. The mean value of the calculated SUHI was studied monthly by the hour. The change in SUHI was investigated at 1:00–1:30 p.m. (post-midday) and 10:00–10:30 p.m. (nighttime). The SUHI alteration from pre-lockdown to lockdown is presented in Fig. 14. This figure shows that the mean SUHI values in March (summer season) increased during the post-midday and nighttime (1:00–1:30 p.m. and 10:00–10:30 p.m.) by approximately 0.278 °C and 4.808 °C, respectively. This is related to the heat emission in hot summer months and air conditioning systems, especially at night. These results align with Chakraborty et al. [20] conducted in north India, which reported that the SUHI increased during the lockdown whilst human activity declined. The aforementioned results are in contrast with the findings of El Kenawy et al. [97], Hidalgo García and Arco Díaz [98], Alqasemi, et al. [99], Cai, et al. [100] and Shikwambana et al. [101], who found that the nighttime SUHI intensity in the Mediterranean and Spanish cities and South Africa decreased during the lockdown. The authors reported that the decline in the nighttime SUHI intensity could be attributed to the improvement in air quality during the lockdown. As such, the increase in nighttime SUHI in the City of Melbourne can be attributed to those air quality parameters whose values increased during the lockdown (UAI and CO). The most significant increase in SUHI values was on 31 March (summertime) during the night (10–10:30 p.m.) (approximately 7.15 °C). The main reason for the increase in the SUHI values is because the initial lockdown stage was on March 27, and many people and retail shopping centers were still using air conditioning systems.

Furthermore, people were still commuting to the city, resulting in anthropogenic heat remaining standard. Evidently, SUHI is a mutual phenomenon with a complex interaction between a wide variety of physical and anthropogenic processes, such as wind speed and relative humidity. El Kenawy et al. [97] highlighted how the dynamics and impacts of SUHI can significantly vary depending on the time of day and type of land and buildings, such as green areas and building material. Further, Chakraborty, et al. [20] proposed that the lockdown-induced anthropogenic pause could potentially affect the natural variability, cloud cover, rainfall, LST, and SUHI.

In this study's examination of the City of Melbourne's lockdown-induced anthropogenic pause, it was apparent that the SUHI value in winter was altered differently compared with that in the summer. During the winter months, the mean SUHI value was negligibly reduced at 1:00–1:30 p.m. (approximately 0.03 °C). By contrast, the mean SUHI value at 10:00–10:30 p.m. increased to approximately 0.417 °C. The most significant increase in the mean SUHI values during winter was observed in July at 10:00–10:30 p.m., which is related to the consumption of a large amount of energy for heating systems in the residential areas.

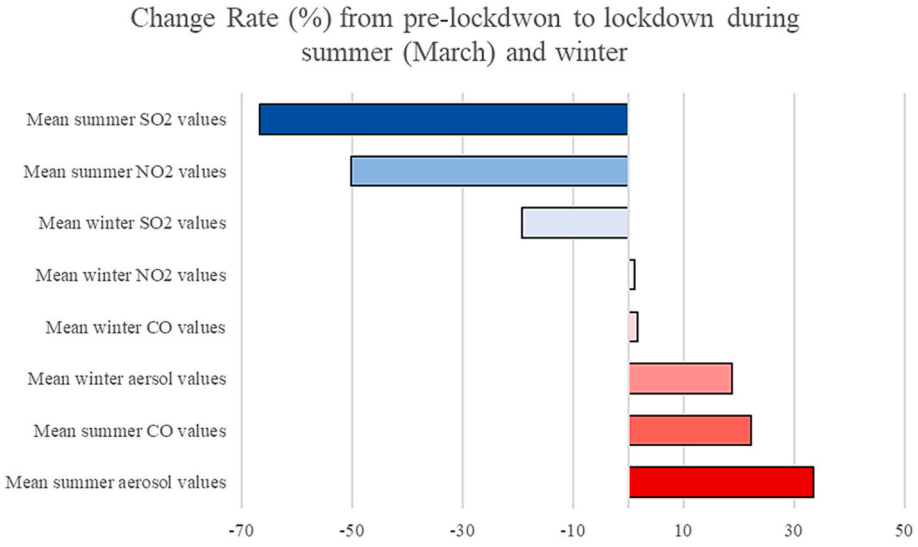


**Fig. 13.** Air quality factor change rate from pre-lockdown to lockdown phase during the summer (March) and winter months (July and August).

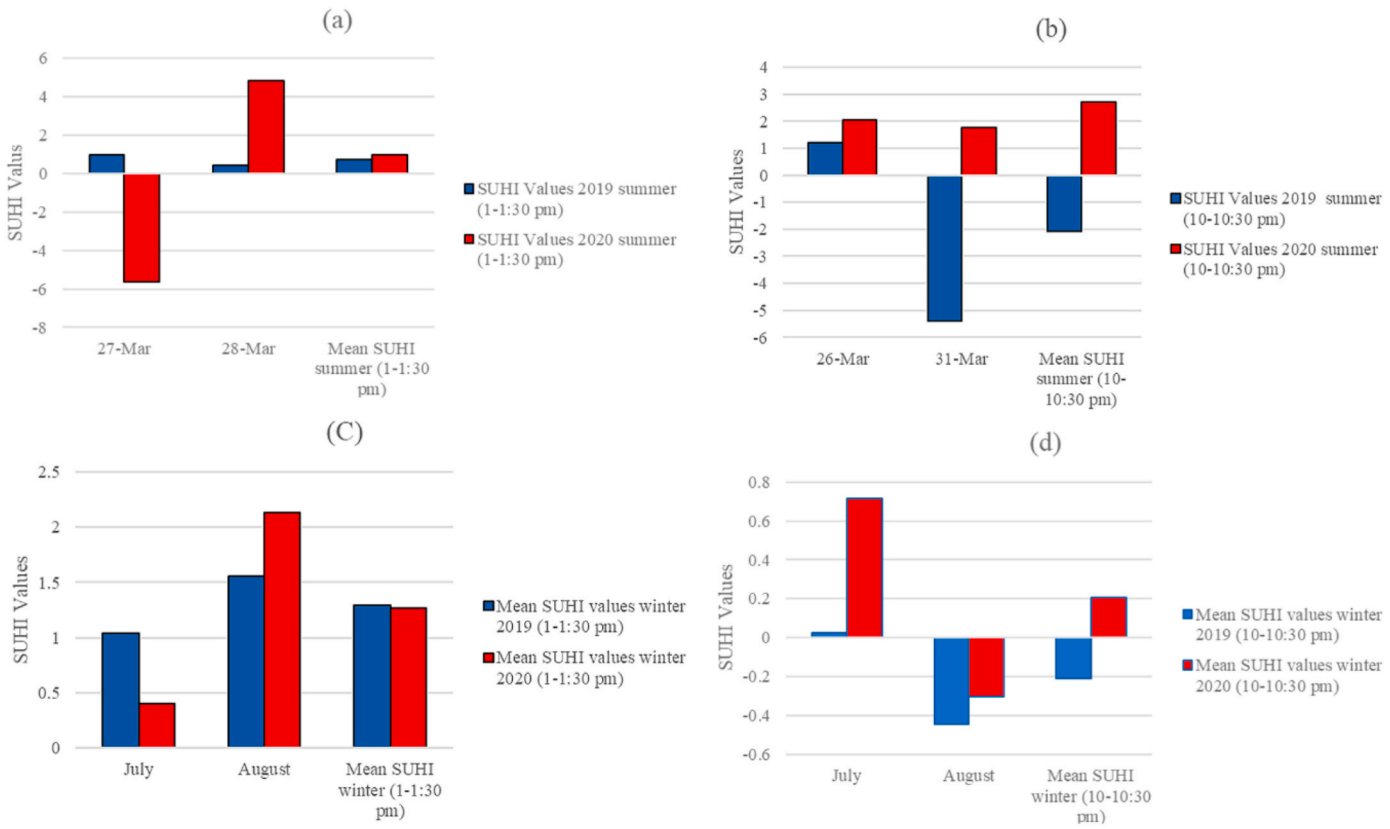


**Fig. 14.** SUHI values (°C) during March the pre-lockdown (2019) and lockdown (2020) at 1:00–1:30 p.m. (a); SUHI values (°C) during March the pre-lockdown (2019) and lockdown (2020) at 10:00–10:30 p.m. (b); mean SUHI values (°C) during the winter pre-lockdown (2019) and lockdown (2020) at 1:00–1:30 p.m. (c), and mean SUHI values (°C) during the winter pre-lockdown (2019) and lockdown (2020) at 10:00–10:30 p.m.) (d).

Fig. 14 shows that the most dominant range of the SUHI value during the summer (1:00–1:30 p.m.) pre-lockdown was between 0.5 °C and 1 °C, covering the inner east areas of the city. The lowest SUHI values at this time were spatially distributed in the east southern, and western areas, where high-rise buildings (CBD) and Fisherman's Bend are located. The highest SUHI values ranged between 2 °C and 2.5 °C and were spatially located in West Footscray, Coode Island, Royal Park, and Flemington Racecourse in the northeastern and western parts of the city.

At the start of the lockdown, the SUHI values during March (1:00–1:30 p.m.) increased in all areas. The high SUHI values during lockdown at 1:00–1:30 p.m. spatially create a cluster that connects the city's inner suburbs to the west (such as West Footscray) and the northwest (such as Kensington) suburbs. These areas are mostly covered by impervious surfaces, causing them to become hotter during summer. Firozjaei et al. [102] showed that the percentage of impervious surfaces could be a suitable factor to indicate the degree of human activity. Increasing the impervious surfaces will reduce the evapotranspiration and increase the LST and SUHI intensity. In fact, more heat can be absorbed during the summertime by impervious surfaces compared with during winter because the sunshine duration is longer, and the direct solar radiation is larger. This situation results in the use of more air-conditioning units for temperature reduction.

Fig. 15 displays that the SUHI values during March's nighttime (10:00–10:30 p.m.) mainly increased in the southeast areas (Docklands Harbor), with a value ranging between 3.5 °C and 5 °C. In addition, the east-side areas that comprise mostly high-rise buildings and shopping centers have lower SUHI values (<1.5 °C). The SUHI values at nighttime (10:00–10:30 p.m.) increased in most parts of the city, except the southeast areas. The highest range of SUHI values (3 °C-4 °C) was spatially distributed in the southeast and west parts of the city. Furthermore, the SUHI value's increment in March (1:00–1:30 p.m.) mostly occurred on the northern side of the city, which is contrary to the increment at 10:00–10:30 p.m., which mainly occurred in the southeast and west areas. The SUHI increment due to lockdown in March (10:00–10:30 and 1:00–1:30 p.m.) was significant in areas with more impervious surfaces.

In wintertime, the highest range of SUHI values (3 °C-3.5 °C) during the pre-lockdown phase (1:00–1:30 p.m.) covered the inner and west sides of the city, similar to during the March lockdown (1:00–1:30 p.m.). Furthermore, most areas covered by the impervious surfaces in the west and high-rise buildings had lower SUHI values during the winter lockdown (1:00–1:30 p.m.) than during the pre-lockdown phase.

The SUHI values in wintertime (10:00–10:30 p.m.) decreased to below 1.5 °C. The SUHI values between 1 °C and 1.5 °C were the most dominant range during the wintertime pre-lockdown (10:00–10:30 p.m.). The lowest SUHI values were mostly scattered on the west and southwest side of the city, where Docklands Wharf and other large-scale impervious surfaces are located. Meanwhile, the SUHI values were slightly higher on the southern east side, where high-rise buildings are located, with values between 1.5 °C and 2 °C. During the winter lockdown (10:00–10:30 p.m.), the SUHI values in the southeast and west areas increased with the rise in energy demand and consumption in residential areas. The SUHI values also increased in the northern parts of the city. However, the alteration was negligible due to the generally cooler weather pattern.

### 4.3. Air temperature

The mean value of the air temperature based on the monthly by-hour ECMWF and ERA5 LAND satellite imageries were calculated to investigate the alteration of the air temperature. The air temperature alterations were investigated at 1:00–1:30 p.m. and 10:00–10:30 p.m.

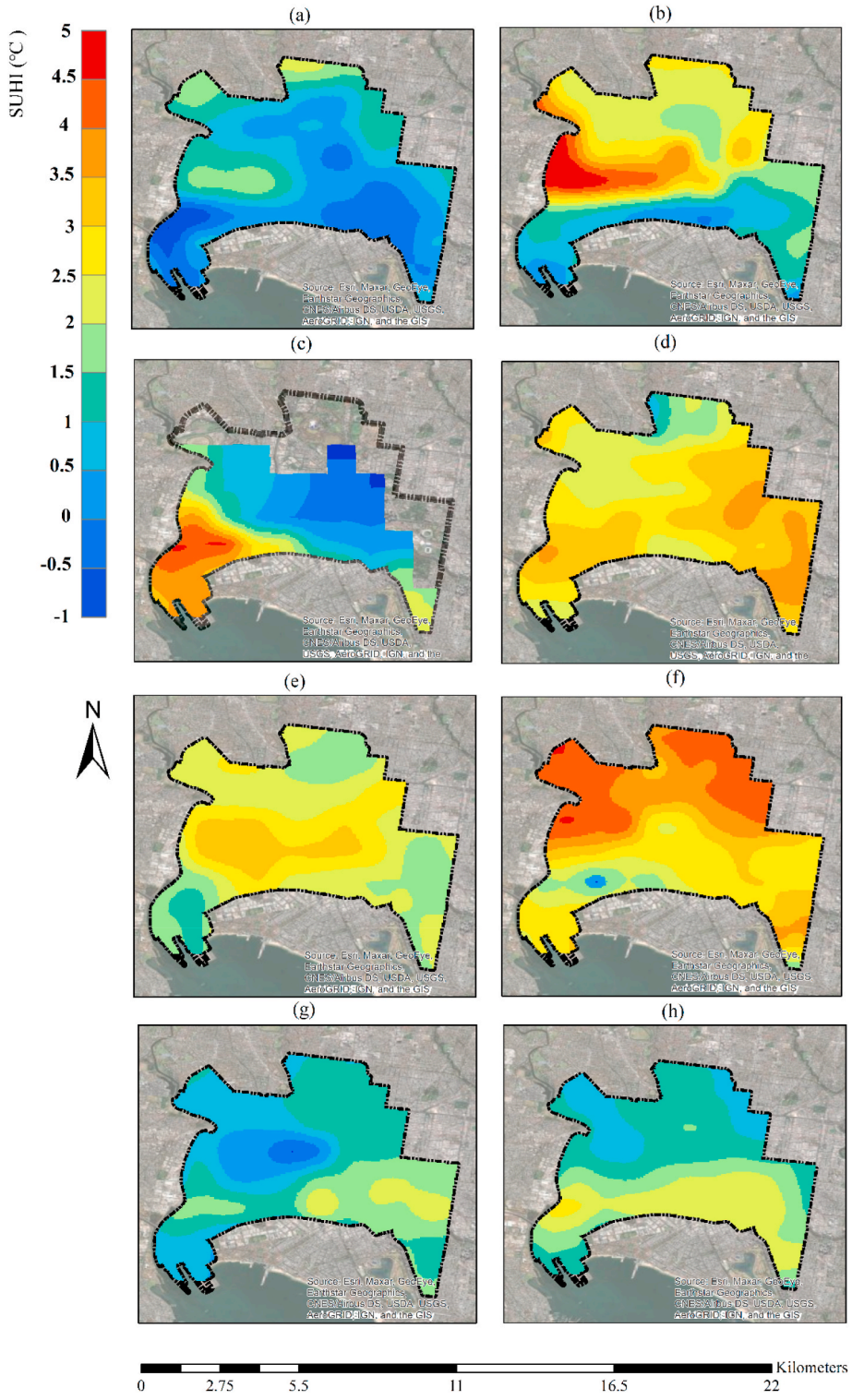


**Fig. 15.** Spatiotemporal distribution of mean SUHI (°C) over the City of Melbourne: (a) March 2019 (pre-lockdown) (1:00–1:30 p.m.), (b) March 2020 (lockdown) (1:00–1:30 p.m.), (c) March 2019 (pre-lockdown) (10:00–10:30 p.m.), (d) March 2020 (lockdown) (10:00–10:30 p.m.), (e) winter 2019 (pre-lockdown) (1:00–1:30 p.m.), (f) winter 2020 (lockdown) (1:00–1:30 p.m.), (g) winter 2019 (pre-lockdown) (10:00–10:30 p.m.) and (h) winter 2020 (lockdown) (10:00–10:30 p.m.).

Fig. 16 indicates that the air temperature in March (pre-lockdown) decreased from 17.92 °C to 16.05 °C at 1:00–1:30 p.m. Furthermore, the air temperature values decreased from 15.62 °C to 14.04 °C at 10:00–10:30 p.m. The decreased air temperature values at 1:00–1:30 p.m. were slightly higher than those at 10:00–10:30 p.m.

Similar to summertime, the air temperature decreased in the winter months from the pre-lockdown to the lockdown phase. The most significant air temperature value drop was in July from 9.42 °C to 8.47 °C. The highest change rate (−12.65%) and air temperature reduction during winter were for the month of July at 10:00–10:30 p.m. The most significant air temperature reduction during the winter and summer months was in July, followed by March.

The City of Melbourne has witnessed a sudden reduction in anthropogenic activities for more than 60 days. The major sources of

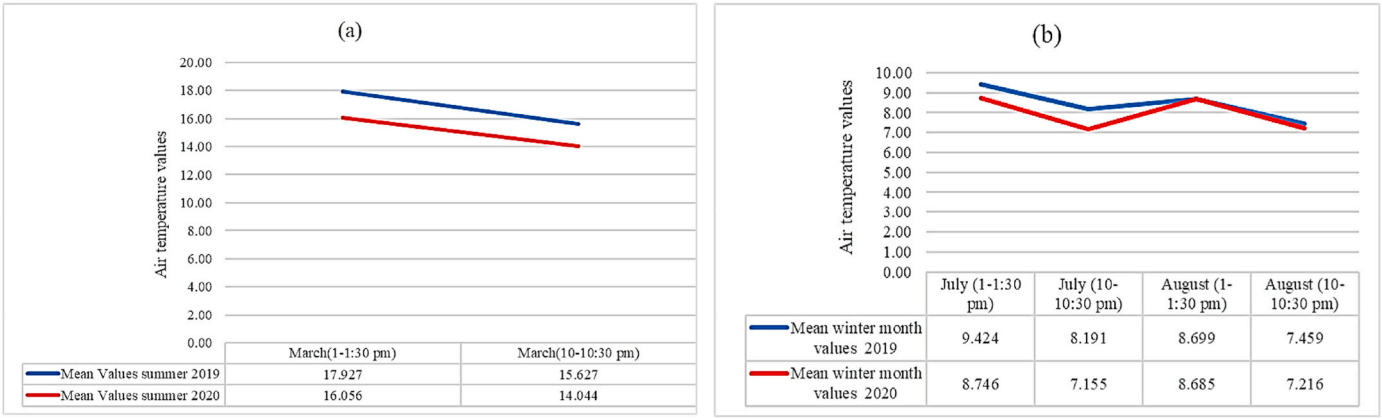


**Fig. 16.** Alteration of the monthly mean air temperature values (°C) for summertime (a) and the monthly mean air temperature (°C) wintertime values (b) during pre-lockdown (2019) and lockdown (2020) at 1:00–1:30 and 10:00–10:30 p.m.

anthropogenic heat are air quality parameters, transport services, industrial activities, and household cooking. Anthropogenic heat is well-known as an effective parameter to represent rising urban temperatures and the shaping of a warm air canopy over the city, thereby increasing the ambient air temperature by several degrees Celsius.

### 4.4. Lighting energy consumption

In this study, the lighting energy consumption analysis was based on the VIIRS nighttime monthly images with s satellite acquisition time of 10:00–10:30 p.m. Fig. 17 presents the alteration of energy consumption.

Fig. 17 indicates that the highest lighting energy consumption during the pre-lockdown and lockdown was in July. However, the lowest lighting energy consumption showed a different situation between the two phases. During the pre-lockdown phase, the lowest lighting energy consumption was in March, while during the lockdown, it was in August.

Furthermore, the highest change rate and reduction in lighting energy consumption from pre-lockdown to lockdown were in August during winter. By contrast, the lowest change rate value and a negligible increase in lighting energy consumption were detected in March.

Fig. 18 reveals that the highest value of lighting energy consumption (52 W) and the dominant range (25–35 W) during the pre-lockdown was spatially distributed on the city's southwest side, which is near West Footscray, the logistics depot, Coode Island, and loading docks. These areas had higher lighting energy consumption values mainly because they consume more lighting than other areas due to safety concerns. During the lockdown, the highest value of the lighting energy consumption increased to 65 W. During the lockdown, the dominant range of energy consumption values (35–45 W) was spatially distributed in the inner parts of the city, where most high-rise buildings and loading docks are located. The difference between pre-lockdown and lockdown energy consumption reflected the shift toward more people staying in their houses during lockdown; accordingly, their consumption rate of lighting energy increased. Furthermore, the highest lighting energy consumption change rate was detected in the northwest portion, where the Flemington Racecourse is located, with the highest consumption during nighttime.

During the winter and pre-lockdown, the highest energy consumption values (>35 W) were mostly spatially distributed on the southeast and west sides, where the high-rise buildings and loading docks are located. Similar to the pre-lockdown, the spatial distribution of the highest lighting energy consumption values (>35 W) was in the southeast and west. However, the total lighting energy consumption was reduced in these areas from pre-lockdown to lockdown.

The change rate values demonstrate that the lighting energy consumption rate mainly was reduced during winter in various areas of the city. Only the areas close to Royal Melbourne Hospital and Woolworths in North Melbourne showed an increase in lighting energy consumption

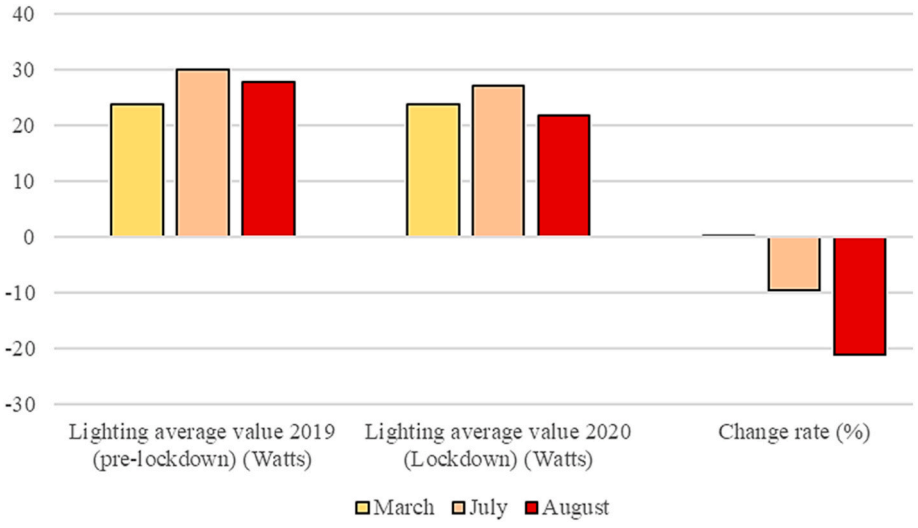


**Fig. 17.** Alteration of the monthly mean lighting energy consumption values (Watts) during the pre-lockdown (2019) and lockdown (2020) phases of the available summer and winter months at 10:00–10:30 p.m.

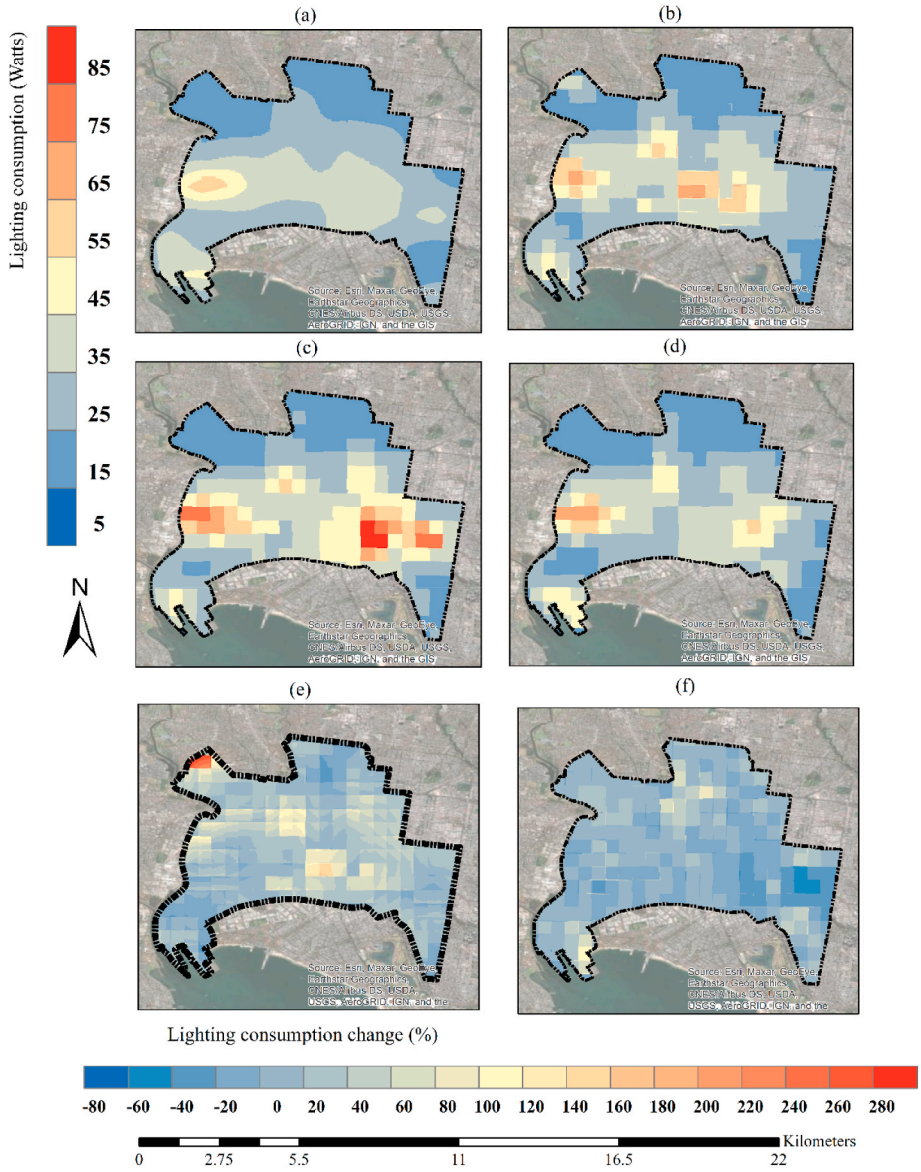


**Fig. 18.** Spatiotemporal distribution of the mean lighting energy consumption (Watts) over the City of Melbourne: (a) March 2019 (pre-lockdown), (b) March 2020 (lockdown), (c) winter 2019 (pre-lockdown), (d) winter 2020 (lockdown), (e) mean lighting energy consumption change rate (%) between pre-lockdown and lockdown during summer and (f) mean lighting energy consumption change rate (%) between pre-lockdown and lockdown during winter.

during winter. The change rate in summer was mostly positive in the inner parts of the city, where most impervious surfaces and built-up areas are located. The increase in lighting energy consumption in summer is in accordance with the findings of the IEA [103] that increased lighting energy consumption occurred in domestic households during lockdowns. In the pre-lockdown phase, many City of Melbourne residents visit shoppingcentres to avoid hot days in summer. However, most residents stayed in their homesmost residents stayed in their homes during the lockdown and used their air-conditioning units during the lockdown. The energy consumption change rate in the winder did not increase in built-up areas because the temperature reduced during the night when people were already at home in the pre-lockdown and lockdown phases.

Similar to Aruga et al. [35], the lockdown in the City of Melbourne had negative effects on lighting energy consumption during summer; however, it plummeted during winter due to the reduced activity level of some industries. The findings from Jiang et al. [36] also exhibit some similarities with this study. For instance, the lighting energy consumption related to renewable energy demand increased during summer and winter in areas where renewable energy products were available; as such, the lighting energy consumption of industrial and commercial areas reduced during the summer lockdown. However, residential lighting energy consumption increased. In winter, the activities required to produce medical products and provide caregiving increased, as observed in the increased lighting energy consumption in that period at Royal Melbourne Hospital.

## 5. Conclusions, limitations, implications, and future studies

This study considered the impact of the COVID-19 lockdowns on air quality factors, SUHI, and lighting energy consumption by investigating the $NO_2$, $SO_2$, CO, UAI, SUHI, and lighting energy consumption levels in the City of Melbourne and evaluating their spatial distribution variations using different satellite imageries. Subsequently, an analysis was conducted to understand the changes from the 2019 pre-lockdown phase to the 2020 lockdown. The findings revealed that the mean $NO_2$, $SO_2$, UAI, air temperature, and SUHI values across the city decreased during the lockdown in summer. Meanwhile, the lighting

energy consumption, SUHI, $SO_2$, UAI, and air temperature decreased during the winter lockdown. The major shifts included the largest average drop in $SO_2$ and $NO_2$ during summer, followed by the increase in UAI and CO throughout the lockdown period compared with the same period in 2019.

This study showed that various locations within the City of Melbourne recorded different findings regarding the major parameters during the summer and winter times of the lockdown and pre-lockdown phases. This study revealed the importance of urban form (such as high-rise buildings on the east side and the industrial areas on the west) and the type of land (mainly the impervious surfaces and urban green spaces) in these differences. Furthermore, satellite data were a significant resource for investigating the air quality, SUHI, air temperature, and lighting energy consumption parameters because of the spatial coverage of the data. This study could be considered a benchmark for city planners and designers for managing air quality, air temperature, SUHI, and lighting energy consumption due to the insights inadvertently revealed by various lockdown restrictions on industrial, residential, and recreational areas. The impact of the COVID-19 pandemic resulted in the emergence of a new baseline of air quality, surface, and air temperature to be used in air pollution and heat mitigation strategies. The COVID-19 lockdowns provided an opportunity to represent how substantially human behaviour can affect air quality and lighting energy consumption. The lockdowns and city dwellers' resultant behavioural change altered lighting energy consumption and air quality. This demonstrated that better strategies influencing human behaviour could make a substantial difference. Several implications can be drawn, with this study generally referring to three fundamental shifts that could be the focus of such strategies:

- Increased adoption of telecommuting/remote work.
- Safe shared mobility, including both public transit and carpooling; and
- De-carbonization of the power sector and transition to clean energy.

Future research should evaluate larger-scale datasets. Examining the impacts of COVID-19 lockdowns shows that reducing lighting energy consumption, even just in specific sectors, could have significant implications for different levels of policy initiatives. Therefore, policy interventions should reflect on the potential for city dwellers to enact behavioural changes while considering the role of socio-economic status.

From another point of view, future studies could consider additional air pollution factors, such as $O_3$, formaldehyde, and other types of $NO_x$, $SO_x$, and COx. In addition, other important and effective factors influencing SUHI and LST, such as land-use patterns and topography, need to be further analyzed to reveal the effect of COVID-19 lockdown emission reductions on anthropogenic heat.

From a methodological point of view, additional data from field calculation methods for air pollution factors and air temperature could be considered to justify the results and solve the spatial and temporal resolution limitation of the satellite imageries. For instance, GIS-based forecasting can estimate the ambient air pollution levels at high temporal and spatial resolutions, leading to the mapping and generation of results for different scenarios. This initiative can be integrated with socio-economic data to gain a better and more comprehensive understanding of air quality parameters.

One of the limitations of this research is the short duration studied, resulting in the deviation of the results from the exact effect of environmental pollution. Thus, future studies could record more days in any upcoming potential lockdown phases.

Further studies can overcome the limitation of the Spatio-temporal resolution of satellite imageries by implementing data fusion and downscaling methods, especially for larger-scale studies conducted on metropolitan areas. Furthermore, future studies could investigate the relationship between the air quality parameters, SUHI, and lighting energy consumption. There is also potential to consider additional interventional parameters, such as meteorological factors, to recognize how they could potentially contribute to the relationship between the SUHI, lighting energy consumption, and air quality factors.

## Credit author statement

**Elmira Jamei:** Conceptualization, Methodology, Writing – original draft preparation **Yashar Jamei.:** Conceptualization, Methodology, Software, Formal analysis, Writing – original draft. **Mehdi Seyedmahmoudian:** Conceptualization, Writing- Reviewing and Editing, Methodology **Ben Horan:** Supervision, Conceptualization, review & editing. **Saad Mekhilef:** Supervision, Conceptualization, review & editing. **Alex Stojcevski:** Supervision. Conceptualization, Writing – review & editing.

## Declaration of competing interest

The authors declare that they have no known competing financial interests or personal relationships that could have appeared to influence the work reported in this paper.

## References


[1] Energy Rating, Lighting Energy Rating, 2021 accessible at https://www.energyrating.gov.au/products/lighting#:~:text=Overview,40%25%20of%20in%20commercial%20premises.

[2] Y. Kikegawa, Y. Genchi, H. Kondo, K. Hanaki, Impacts of city-block-scale countermeasures against urban heat-island phenomena upon a building's energy-consumption for air-conditioning, Appl. Energy 83 (6) (2006/06/01/2006) 649–668, https://doi.org/10.1016/j.apenergy.2005.06.001.

[3] H. Fonseka, H. Zhang, Y. Sun, H. Su, H. Lin, Y. Lin, Urbanization and its impacts on land surface temperature in Colombo metropolitan area, Sri Lanka, from 1988 to 2016, Rem. Sens. 11 (8) (2019) 957.

[4] Z. Chao, A.I. van Dijk, L. Wang, M. Che, S. Hou, Effects of different urbanization levels on land surface temperature change: taking tokyo and Shanghai for example, Rem. Sens. 12 (12) (2020) 2022.

[5] X. Gui, L. Wang, R. Yao, D. Yu, Investigating the urbanization process and its impact on vegetation change and urban heat island in Wuhan, China, Environ. Sci. Pollut. Control Ser. 26 (30) (2019) 30808–30825.

[6] IEA, *Multiple Benefits of Energy Efficiency*, Paris, 2019 accessible at https://www.iea.org/reports/multiple-benefits-of-energy-efficiency Energy efficiency market report.

[7] WHO, WHO Announces COVID-19 Outbreak a Pandemic, World Health Organization, 2020 accessible at, http://www.euro.who.int/en/health-topics/health-emergencies/coronavirus-covid-19/news/news/2020/3/who-announces-covid-19-outbreak-apandemic.

[8] C. Potter, O. Alexander, Impacts of the San Francisco Bay Area shelter-in-place during the COVID-19 pandemic on urban heat fluxes, Urban Clim. 37 (2021), 100828.

[9] M. McCarthy, C. Harpham, C. Goodess, P. Jones, Simulating climate change in UK cities using a regional climate model, HadRM3, Int. J. Climatol. 32 (12) (2012) 1875–1888.

[10] X.-L. Chen, H.-M. Zhao, P.-X. Li, Z.-Y. Yin, Remote sensing image-based analysis of the relationship between urban heat island and land use/cover changes, Remote Sens. Environ. 104 (2) (2006/09/30/2006) 133–146, https://doi.org/10.1016/j.rse.2005.11.016.

[11] City of Melbourne, COVID-19 Reactivation and Recoverty Plan. City of the Future, September 2020 accessible at https://www.melbourne.vic.gov.au/sitecollectiondocuments/covid-19-reactivation-recovery-plan.pdf.

[12] VictoriaStateGovernment. "Air pollution." Victoria State Government, Department of Health, Health Protection, Environmental Health Unit , 2021 accessible at https://www.betterhealth.vic.gov.au/health/healthyliving/air-pollution#bhc-content.

[13] M.B. Karuppasamy, et al., Air pollution improvement and mortality rate during COVID-19 pandemic in India: global intersectional study, Air Quality, Atmosphere & Health 13 (11) (2020) 1375–1384.

[14] H. Li, X.-L. Xu, D.-W. Dai, Z.-Y. Huang, Z. Ma, Y.-J. Guan, Air pollution and temperature are associated with increased COVID-19 incidence: a time series study, Int. J. Infect. Dis. 97 (2020) 278–282.

[15] L. Li, et al., Air quality changes during the COVID-19 lockdown over the Yangtze River Delta Region: an insight into the impact of human activity pattern changes on air pollution variation, Sci. Total Environ. 732 (2020), 139282.

[16] B.R. Parida, S. Bar, D. Kaskaoutis, A.C. Pandey, S.D. Polade, S. Goswami, Impact of COVID-19 induced lockdown on land surface temperature, aerosol, and urban heat in Europe and North America, Sustain. Cities Soc. 75 (2021), 103336.

[17] D. Nanda, D.R. Mishra, D. Swain, COVID-19 lockdowns induced land surface temperature variability in mega urban agglomerations in India, Environ. Sci. J. Integr. Environ. Res.: Process. Impacts 23 (1) (2021) 144–159.

[18] D.H. García, J.A. Díaz, Impacts of the COVID-19 confinement on air quality, the Land Surface Temperature and the urban heat island in eight cities of Andalusia (Spain), Remote Sens. Appl.: Soc. Environ. 25 (2022), 100667.

[19] Z. Liu, et al., Urban heat islands significantly reduced by COVID-19 lockdown, Geophys. Res. Lett. 49 (2) (2022) e2021GL096842.

[20] T. Chakraborty, C. Sarangi, X. Lee, Reduction in human activity can enhance the urban heat island: insights from the COVID-19 lockdown, Environ. Res. Lett. 16 (5) (2021), 054060.

[21] K. Fuladlu, H. Altan, Examining land surface temperature and relations with the major air pollutants: a remote sensing research in case of Tehran, Urban Clim. 39 (2021), 100958.

[22] K. Nakajima, Y. Takane, Y. Kikegawa, Y. Furuta, H. Takamatsu, Human behaviour change and its impact on urban climate: restrictions with the G20 Osaka Summit and COVID-19 outbreak, Urban Clim. 35 (2021), 100728.

[23] G. Roshan, R. Sarli, J.M. Fitchett, Urban heat island and thermal comfort of Esfahan City (Iran) during COVID-19 lockdown, J. Clean. Prod. (2022/03/31/ 2022), 131498, https://doi.org/10.1016/j.jclepro.2022.131498.

[24] H.Z. Hadibasyir, S.S. Rijal, D.R. Sari, Comparison of land surface temperature during and before the emergence of covid-19 using modis imagery in Wuhan city, China, Forum Geografi 34 (1) (2020) 1–15.

[25] Q. Liu, et al., Spatiotemporal patterns of COVID-19 impact on human activities and environment in mainland China using nighttime light and air quality data, Rem. Sens. 12 (10) (2020) 1576 [Online]. Available: https://www.mdpi.com/2072-4292/12/10/1576.

[26] D. Rodríguez-Urrego, L. Rodríguez-Urrego, Air quality during the COVID-19: PM2. 5 analysis in the 50 most polluted capital cities in the world, Environ. Pollut. 266 (2020), 115042.

[27] W. Ming, Z. Zhou, H. Ai, H. Bi, Y. Zhong, COVID-19 and air quality: evidence from China, Emerg. Mark. Finance Trade 56 (10) (2020) 2422–2442.

[28] S. Gautam, The influence of COVID-19 on air quality in India: a boon or inutile, Bull. Environ. Contam. Toxicol. 104 (6) (2020) 724–726.

[29] S. Zangari, D.T. Hill, A.T. Charette, J.E. Mirowsky, Air quality changes in New York City during the COVID-19 pandemic, Sci. Total Environ. 742 (2020), 140496.

[30] M.G. Adam, P.T. Tran, R. Balasubramanian, Air quality changes in cities during the COVID-19 lockdown: a critical review, Atmos. Res. 264 (2021), 105823.

[31] P. Kumari, D. Toshniwal, Impact of lockdown on air quality over major cities across the globe during COVID-19 pandemic, Urban Clim. 34 (2020), 100719.

[32] L. Menut, B. Bessagnet, G. Siour, S. Mailler, R. Pennel, A. Cholakian, Impact of lockdown measures to combat Covid-19 on air quality over western Europe, Sci. Total Environ. 741 (2020), 140426.

[33] M. Filonchyk, V. Hurynovich, H. Yan, Impact of covid-19 lockdown on air quality in the Poland, eastern europe, Environ. Res. 198 (2021), 110454.

[34] H. Kang, J. An, H. Kim, C. Ji, T. Hong, S. Lee, Changes in energy consumption according to building use type under COVID-19 pandemic in South Korea, Renew. Sustain. Energy Rev. 148 (2021), 111294.

[35] K. Aruga, M. Islam, A. Jannat, Effects of COVID-19 on Indian energy consumption, Sustainability 12 (14) (2020) 5616.

[36] P. Jiang, Y. Van Fan, J.J. Klemeš, Impacts of COVID-19 on energy demand and consumption: challenges, lessons and emerging opportunities, Appl. Energy 285 (2021), 116441.

[37] J. Rouleau, L. Gosselin, Impacts of the COVID-19 lockdown on energy consumption in a Canadian social housing building, Appl. Energy 287 (2021), 116565.

[38] Q. Wang, S. Li, F. Jiang, Uncovering the impact of the COVID-19 pandemic on energy consumption: new insight from difference between pandemic-free scenario and actual electricity consumption in China, J. Clean. Prod. 313 (2021), 127897.

[39] M. Carvalho, D. Bandeira de Mello Delgado, K.M. de Lima, M. de Camargo Cancela, C.A. dos Siqueira, D.L.B. de Souza, Effects of the COVID-19 pandemic on the Brazilian electricity consumption patterns, Int. J. Energy Res. 45 (2) (2021) 3358–3364.

[40] City of Melbourne. "Melbourne profile." City of Melbourne, 2022 accessible at https://www.melbourne.vic.gov.au/about-melbourne/melbourne-profile.

[41] A.P. Sturman, N.J. Tapper, The Weather and Climate of Australia and New Zealand, Oxford University Press, USA, 1996.

[42] DHHS. Victora. "Coronavirus update for Victoria", Victoria State Government, 30 october 2020 accessible at https://www.dhhs.vic.gov.au/coronavirus-update-victoria-30-october-2020.

[43] Alan Oster, et al., NAB's Group Economics, Impact of COVID-19 on Australia's CBD's & what Would Encourage Us to Visit More Often?. NAB Consumer Insight Report NAB, Australia, 2021. In press.

[44] R. Millar. "To CBD or not to CBD? COVID's question for the future of Melbourne." The Age, 2021 accessible at https://www.theage.com.au/national/victoria/to-cbd-or-not-to-cbd-covid-s-question-for-the-future-of-melbourne-20210603-p57xqj.html.

[45] S. Lolli, Y.-C. Chen, S.-H. Wang, G. Vivone, Impact of meteorological conditions and air pollution on COVID-19 pandemic transmission in Italy, Sci. Rep. 10 (1) (2020) 1–15.

[46] BOM. "Meteorological parameters of Melbourne olypmic park weather station.". Bureau Meteorology, 2020 accessible at https://www.willyweather.com.au/climate/weather-stations/vic/melbourne/melbourne-olympic-park.html?superGraph=plots:temperature,humidity,wind-speed,rainfall,grain:daily,startDate:2020-07-01,endDate:2020-08-31&climateRecords=period:all-time&longTermGraph=plots:temperature,period:all-time,month:3&windRose=period:5-year,month:all-months.

[47] G.C. Hulley, S.J. Hook, C. Hughes, MODIS MOD21 Land Surface Temperature and Emissivity Algorithm Theoretical Basis Document, Jet Propulsion Laboratory, National Aeronautics and Space, Pasadena, CA, 2012. In press.

[48] L. Veci, P. Prats-Iraola, R. Scheiber, F. Collard, N. Fomferra, M. Engdahl, The sentinel-1 toolbox, in: Proceedings of the IEEE International Geoscience and Remote Sensing Symposium (IGARSS), IEEE, 2014, pp. 1–3.

[49] E. Sentinel, "User handbook," ESA Standard Document, vol. 64.

[50] T.G. Farr, et al., The shuttle radar topography mission, Rev. Geophys. 45 (2) (2007).

[51] L.-W. Hung, S.J. Anderson, A. Pipkin, K. Fristrup, Changes in night sky brightness after a countywide LED retrofit, J. Environ. Manag. 292 (2021), 112776.

[52] S. Mills, S. Weiss, C. Liang, VIIRS day/night band (DNB) stray light characterization and correction, in: Earth Observing Systems XVIII, vol. 8866, International Society for Optics and Photonics, 2013, p. 88661P.

[53] J. Muñoz-Sabater, et al., ERA5-Land: a state-of-the-art global reanalysis dataset for land applications, Earth Syst. Sci. Data Discuss. (2021) 1–50.

[54] Siddans Richard, Smith Andy, TROPOMI-SENTINEL 5 P, Sentinel-5 precursor/ TROPOMI Level 2 Product User Manual NPP Cloud, RAL Space (1.0.1) (2018). https://sentinel.esa.int/documents/247904/2474726/Sentinel-5P-Level-2-Product-User-Manual-NPP-Cloud-product.

[55] J. Veefkind, et al., TROPOMI on the ESA Sentinel-5 Precursor: a GMES mission for global observations of the atmospheric composition for climate, air quality and ozone layer applications, Remote Sens. Environ. 120 (2012) 70–83.

[56] Z.S. Venter, K. Aunan, S. Chowdhury, J. Lelieveld, COVID-19 lockdowns cause global air pollution declines, Proc. Natl. Acad. Sci. USA 117 (32) (2020) 18984–18990.

[57] D. Griffin, et al., High-resolution mapping of nitrogen dioxide with TROPOMI: first results and validation over the Canadian oil sands, Geophys. Res. Lett. 46 (2) (2019) 1049–1060.

[58] A. Lorente, et al., Quantification of nitrogen oxides emissions from build-up of pollution over Paris with TROPOMI, Sci. Rep. 9 (1) (2019) 1–10.

[59] T. E. S. Agency. "Sentinel-5P TROPOMI user guide." Copernicus, 2021 accessible at https://sentinel.esa.int/web/sentinel/user-guides/sentinel-5p-tropomi.

[60] Z. Wan, Collection-6 MODIS Land Surface Temperature Products Users' Guide, ICESS, University of California, Santa Barbara, 2013.

[61] W. Wang, S. Liang, T. Meyers, Validating MODIS land surface temperature products using long-term nighttime ground measurements, Remote Sens. Environ. 112 (3) (2008) 623–635.

[62] Z. Sun, R. Xu, W. Du, L. Wang, D. Lu, High-resolution urban land mapping in China from sentinel 1A/2 imagery based on Google Earth engine, Rem. Sens. 11 (7) (2019) 752 [Online]. Available: https://www.mdpi.com/2072-4292/11/7/752.

[63] I.D. Stewart, Redefining the Urban Heat Island, University of British Columbia, 2011.

[64] R. Yao, L. Wang, X. Huang, W. Gong, X. Xia, Greening in rural areas increases the surface urban heat island intensity, Geophys. Res. Lett. 46 (4) (2019) 2204–2212.

[65] E. Meriman. "Dynamically quantifying the urban heat island effect, 2019 accessible at https://mediaspace.esri.com/media/t/1_tz92yluw.

[66] N. Zhao, et al., Time series analysis of VIIRS-DNB nighttime lights imagery for change detection in urban areas: a case study of devastation in Puerto Rico from hurricanes Irma and Maria, Appl. Geogr. 120 (2020), 102222.

[67] C. Small, C.D. Elvidge, K. Baugh, Mapping urban structure and spatial connectivity with VIIRS and OLS night light imagery, in: Joint Urban Remote Sensing Event, vol. 2013, IEEE, 2013, pp. 230–233.

[68] T. Ma, Z. Yin, A. Zhou, Delineating spatial patterns in human settlements using VIIRS nighttime light data: a watershed-based partition approach, Rem. Sens. 10 (3) (2018) 465.

[69] G. Falchetta, M. Noussan, Interannual variation in night-time light radiance predicts changes in national electricity consumption conditional on income-level and region, Energies 12 (3) (2019) 456.

[70] H. Zhu, P. Blackborow, Understanding Radiance (Brightness), Irradiance and Radiant Flux, Woburn, MA, 2011.

[71] PNGK, Nightlight Conversion, PNGK, 2021. In press, https://pngk.org/.

[72] R.G. Ryan, J.D. Silver, R. Schofield, Air quality and health impact of 2019–20 Black Summer megafires and COVID-19 lockdown in Melbourne and Sydney, Australia, Environ. Pollut. 274 (2021), 116498.

[73] BOM, Greater Melbourne in March 2019: Warm Days and Nights, Bureau of Meteorology, 2019 accessed, http://www.bom.gov.au/climate/current/month/vic/archive/201903.melbourne.shtml.

[74] BOM, Greater Melbourne in March 2020: Cool Days, Wetter than Average, Bureau of Meteorology, 2020 accessed, http://www.bom.gov.au/climate/current/month/vic/archive/202003.melbourne.shtml.

[75] R. Cichowicz, G. Wielgosiński, W. Fetter, Dispersion of atmospheric air pollution in summer and winter season, Environ. Monit. Assess. 189 (12) (2017) 1–10.

[76] N. Talbot, A. Takada, A.H. Bingham, D. Elder, S.L. Yee, N.E. Golubiewski, An investigation of the impacts of a successful COVID-19 response and meteorology on air quality in New Zealand, Atmos. Environ. 254 (2021), 118322.

[77] H. Patel, N. Talbot, J. Salmond, K. Dirks, S. Xie, P. Davy, Implications for air quality management of changes in air quality during lockdown in Auckland (New Zealand) in response to the 2020 SARS-CoV-2 epidemic, Sci. Total Environ. 746 (2020), 141129.

[78] N. Talbot, R. Lehn, The Impacts of Transport Emissions on Air Quality in Auckland's City Centre, Auckland Council, 2018.

[79] T. Borsdorff, J. Aan de Brugh, H. Hu, I. Aben, O. Hasekamp, J. Landgraf, Measuring carbon monoxide with TROPOMI: first results and a comparison with ECMWF-IFS analysis data, Geophys. Res. Lett. 45 (6) (2018) 2826–2832.

[80] I.Y. Hernández-Paniagua, et al., Impact of the COVID-19 lockdown on air quality and resulting public health benefits in the Mexico city metropolitan area, Front. Public Health 9 (2021) 242.
[81] E. Tello-Leal, B.A. Macías-Hernández, Association of environmental and meteorological factors on the spread of COVID-19 in Victoria, Mexico, and air quality during the lockdown, Environ. Res. 196 (2021), 110442.
[82] M. Zhou, J. Jiang, B. Langerock, B. Dils, M.K. Sha, M. De Mazière, Change of CO concentration due to the COVID-19 lockdown in China observed by surface and satellite observations, Rem. Sens. 13 (6) (2021) 1129.
[83] City of Melbourne, Emissions Reduction Plan for Council Operations (2021-2026), Emissions Reduction Plan - City of Melbourne (2021). In press, https://www.melbourne.vic.gov.au/SiteCollectionDocuments/emissions-reduction-plan-2021-26.pdf.
[84] C. Helfter, et al., Spatial and temporal variability of urban fluxes of methane, carbon monoxide and carbon dioxide above London, UK, Atmos. Chem. Phys. 16 (16) (2016) 10543–10557.
[85] J. Amorim, V. Rodrigues, R. Tavares, J. Valente, C. Borrego, CFD modelling of the aerodynamic effect of trees on urban air pollution dispersion, Sci. Total Environ. 461 (2013) 541–551.
[86] S. Zheng, X. Zhou, R.P. Singh, Y. Wu, Y. Ye, C. Wu, The spatiotemporal distribution of air pollutants and their relationship with land-use patterns in Hangzhou city, China, Atmosphere 8 (6) (2017) 110.
[87] A. Makhelouf, Impact assessment of the construction of tall buildings in a big town on the urban climate and the air pollution, J. Environ. Res. Manag. 3 (4) (2012) 64–74.
[88] H. Abdullahi, G. K. Sinniah, and H. C. Siong, "Urban Growth Air Pollution, CO, NO2 and SO2 Emission and COVID-19 in Kano Metropolis Nigeria".
[89] O. Torres, et al., Aerosols and surface UV products from Ozone Monitoring Instrument observations: an overview, J. Geophys. Res. Atmos. 112 (D24) (2007).
[90] S. Kumar, Effect of meteorological parameters on spread of COVID-19 in India and air quality during lockdown, Sci. Total Environ. 745 (2020), 141021.
[91] X. Chi, J. Hua, S. Hua, X. Ren, S. Yang, Assessing the impacts of human activities on air quality during the COVID-19 pandemic through case analysis, Atmosphere 13 (2) (2022) 181 [Online]. Available: https://www.mdpi.com/2073-4433/13/2/181.
[92] WMO. "World meteorological organization (WMO)-Aerosols, 2021 accessible at " WMO. https://public.wmo.int/en/our-mandate/focus-areas/environment/aerosols.
[93] Q. Xie, Q. Sun, Monitoring the spatial variation of aerosol optical depth and its correlation with land use/land cover in Wuhan, China: a perspective of urban planning, Int. J. Environ. Res. Publ. Health 18 (3) (2021) 1132.
[94] T.R. Oke, The energetic basis of the urban heat island, Q. J. R. Meteorol. Soc. 108 (455) (1982) 1–24.
[95] H. Li, et al., Interaction between urban heat island and urban pollution island during summer in Berlin, Sci. Total Environ. 636 (2018/09/15/2018) 818–828, https://doi.org/10.1016/j.scitotenv.2018.04.254.
[96] J. Crawford, D.D. Cohen, S.D. Chambers, A.G. Williams, A. Atanacio, Impact of aerosols of sea salt origin in a coastal basin: Sydney, Australia, Atmos. Environ. 207 (2019) 52–62.
[97] A.M. El Kenawy, et al., The impact of COVID-19 lockdowns on surface urban heat island changes and air-quality improvements across 21 major cities in the Middle East, Environ. Pollut. 288 (2021), 117802.
[98] D. Hidalgo García, J. Arco Díaz, Impacts of the COVID-19 confinement on air quality, the Land Surface Temperature and the urban heat island in eight cities of Andalusia (Spain), Remote Sens. Appl.: Soc. Environ. 25 (2022/01/01/2022), 100667, https://doi.org/10.1016/j.rsase.2021.100667.
[99] A.S. Alqasemi, M.E. Hereher, G. Kaplan, A.M.F. Al-Quraishi, H. Saibi, Impact of COVID-19 lockdown upon the air quality and surface urban heat island intensity over the United Arab Emirates, Sci. Total Environ. 767 (2021), 144330.
[100] Z. Cai, Y. Tang, Q. Zhan, A cooled city? Comparing human activity changes on the impact of urban thermal environment before and after city-wide lockdown, Build. Environ. 195 (2021), 107729.
[101] L. Shikwambana, M. Kganyago, P. Mhangara, Temporal analysis of changes in anthropogenic emissions and urban heat islands during COVID-19 restrictions in Gauteng province, South Africa, Aerosol Air Qual. Res. 21 (2021), 200437.
[102] M.K. Firozjaei, Q. Weng, C. Zhao, M. Kiavarz, L. Lu, S.K. Alavipanah, Surface anthropogenic heat islands in six megacities: an assessment based on a triple-source surface energy balance model, Remote Sens. Environ. 242 (2020), 111751.
[103] IEA, International Energy Agency, COVID-19 Impact on Electricity, 2020 [Online]. Available: https://www.iea.org/reports/covid-19-impact-on-electricity.